

**Interdiffusion of Bismuth and Zinc in Liquid Tin &
The Effect of Capillary Diameter on the Diffusion Coefficient**

by

Christopher Brock Porth

A thesis submitted to the Faculty of Graduate Studies of

The University of Manitoba

in partial fulfillment of the requirements for the degree of

Master of Science

Department of Mechanical and Manufacturing Engineering

University of Manitoba

Winnipeg, Manitoba, Canada

Copyright © 2008 by Christopher Brock Porth

THE UNIVERSITY OF MANITOBA
FACULTY OF GRADUATE STUDIES

COPYRIGHT PERMISSION

**Interdiffusion of Bismuth and Zinc in Liquid Tin &
The Effect of Capillary Diameter on the Diffusion Coefficient**

BY

Christopher Brock Porth

**A Thesis/Practicum submitted to the Faculty of Graduate Studies of The University of
Manitoba in partial fulfillment of the requirement of the degree
Of
MASTER OF SCIENCE**

Christopher Brock Porth © 2008

Permission has been granted to the University of Manitoba Libraries to lend a copy of this thesis/practicum, to Library and Archives Canada (LAC) to lend a copy of this thesis/practicum, and to LAC's agent (UMI/ProQuest) to microfilm, sell copies and to publish an abstract of this thesis/practicum.

This reproduction or copy of this thesis has been made available by authority of the copyright owner solely for the purpose of private study and research, and may only be reproduced and copied as permitted by copyright laws or with express written authorization from the copyright owner.

ACKNOWLEDGMENTS

The author wishes to acknowledge the financial support of the National Sciences and Engineering Research Council of Canada, and the Engineering Materials Laboratory within the Department of Mechanical and Manufacturing Engineering, at the University of Manitoba. In addition, the author wishes to express sincere gratitude to Professor J. R. Cahoon for his guidance, expertise, and patience throughout the course of this research. And finally, special thanks to Irwin Penner, whose technical knowledge and assistance was greatly appreciated.

ABSTRACT

In this thesis, coefficients for the interdiffusion of Bismuth and Zinc in Liquid Tin were determined using the long capillary technique, and the effect of capillary diameter size on the diffusion coefficient was investigated. The thin-film-disk-at-one-end solution of the diffusion equation was used to determine the interdiffusion coefficients produced from 1.6 mm, 0.8 mm, and 0.5 mm graphite capillaries. Concentration versus distance profiles were obtained using a JEOL 9000 Scanning Electron Microscope (SEM) equipped with an Oxford Instruments Energy Dispersive Spectrometer (EDS). From the experimental dataset, it was shown that decreasing capillary diameter both reduced error and lowered the diffusion coefficient obtained from diffused specimens. The 0.5 mm capillary diameter proved optimum for experimentation, specifically at elevated temperatures. The interdiffusion coefficient of Bi in Sn as determined by this study, expressed in terms of the Arrhenius relationship is given by $D_{Bi-Sn} = 11.56 \pm 2.39 \times 10^{-8} \exp(- (2.29 \pm 0.74) / RT) \text{ m}^2/\text{s}$. Similarly, the interdiffusion for Zn in Sn is given by $D_{Zn-Sn} = 1.34 \pm 0.83 \times 10^{-8} \exp(- (6.86 \pm 3.17) / RT) \text{ m}^2/\text{s}$. Examination of the Arrhenius profiles produced by this research revealed that both Bi and Zn diffuse in Sn at a slower rate than Sn solvent self diffusion. In addition, examination of the experimental data set of both Bi in Sn and Zn in Sn suggests that the diffusion coefficient may not be predicated on simple temperature dependence in at least some liquid alloy metals, and that the diffusion coefficient may be affected by phase transformations or some other structural change occurring within the liquid.

TABLE OF CONTENTS

1	INTRODUCTION	1
2	LITERATURE REVIEW	3
2.1	Fick's Laws	3
2.1.1	The Flux Equation – Fick's First Law	3
2.1.2	The Diffusion Equation – Fick's Second Law.....	4
2.2	The Diffusion Equation - Solutions	6
2.2.1	Solution for Constant D	6
2.2.1.1	The Thin-Film Solution	6
2.2.2	Solution for Variable D.....	10
2.2.2.1	Boltzmann Transformation and the Matano Analysis	10
2.2.3	Finite Difference Numerical Solution.....	13
2.3	Liquid Metal Diffusion Theory	14
2.3.1	Hole Theory	14
2.3.2	Fluctuation Theory	15
2.3.3	Vibrational and Molecular Friction Models.....	16
2.3.4	Viscosity Based Theories.....	16
2.3.5	Sphere Models.....	18
2.4	Liquid Metal Diffusion Experimental Techniques	20
2.4.1	The Long Capillary Method.....	20
2.4.2	The Capillary Reservoir Method.....	21
2.4.3	The Shear Cell Method	22

2.5	The Effect of Capillary Diameter on the Diffusion Coefficient	24
2.6	Diffusion Investigations from Literature	28
2.6.1	Solvent Self Diffusion of Liquid Tin	28
2.6.2	Bismuth in Tin Interdiffusion	29
2.6.3	Zinc in Tin Interdiffusion.....	32
3	EXPERIMENTAL METHODS.....	34
3.1	Apparatus	34
3.1.1	Material Specifications	34
3.1.2	Capillaries	34
3.1.3	Vacuum Furnace	35
3.1.4	Analytical Equipment	36
3.2	Procedure	37
3.2.1	Diffusion Couple Preparation	37
3.2.2	Diffusion Anneal.....	37
3.2.3	Sample Preparation	38
3.2.4	Chemical Analysis	38
3.2.5	Numerical Analysis.....	39
3.2.5.1	The Thin-film Solution – Disk at One End Equation	39
3.2.5.2	Data Normalization	41
3.2.5.3	The Experimental Diffusion Coefficient.....	41
3.2.5.4	Limits of Error	42
4	EXPERIMENTAL RESULTS.....	44
4.1	Bismuth in Tin – Summary of Experimental Data	45

4.2	Zinc in Tin - Summary of Experimental Data	48
5	DISCUSSION.....	49
5.1	Arrhenius Analysis.....	49
5.2	Tin Solvent Self Diffusion – A Comparison of Best Fit Experimental Data.....	52
5.3	Experimental Data Series - A Comparison with Literature	54
5.4	The Effect of Capillary Diameter on the Diffusion Coefficient	57
5.5	Scaling and Numerical Analysis	62
5.6	Possibility of a Liquid Phase Transformation.....	65
6	CONCLUSIONS.....	66
7	RECOMMENDATIONS FOR FUTURE WORK.....	68
8	REFERENCES	69
9	APPENDIX A – Complete Experimental Dataset.....	75
10	APPENDIX B – Select Physical Properties of Tin, Zinc and Bismuth.....	79
10.1	Tin – Select Physical Properties.....	79
10.2	Bismuth – Select Physical Properties.....	82
10.3	Zinc – Select Physical Properties.....	83
10.4	Bismuth-Tin Binary Phase Diagram	84
10.5	Tin-Zinc Binary Phase Diagram	85

LIST OF FIGURES

Figure 1. A graphical representation of the relationship between concentration, flux, and element of incremental distance.....	4
Figure 2. Concentration profiles before and after diffusion for the thin-film solution of the diffusion equation.....	8
Figure 3. An example of a Boltzmann-Matano concentration versus distance diffusion plot.	12
Figure 4. A diagram of a long capillary.	20
Figure 5. Schematic of a shear cell apparatus, showing the stages of shear: initial, aligned, and final position.....	23
Figure 6. A long capillary liquid diffusion specimen orientated vertically within a furnace, subjected to a horizontal temperature gradient.	27
Figure 7. Arrhenius plot for the solvent self-diffusion of Sn.	28
Figure 8. Bi in Sn – Summary of interdiffusion studies from literature.....	29
Figure 9. Zn in Sn – Summary of interdiffusion studies from literature.....	32
Figure 10. A schematic of the experimental apparatus utilized in this research.	36
Figure 11. Arrhenius plot for the interdiffusion of Bi in liquid Sn.	49
Figure 12. Arrhenius plot for the interdiffusion of Zn in liquid Sn.....	50
Figure 13. Comparison of 0.5-mm Bi in Sn Experimental Results and Best Fit Sn Solvent Self-Diffusion Data.....	52
Figure 14. Comparison of 0.5-mm Zn in Sn Experimental Results and Best Fit Sn Solvent Self-Diffusion Data.....	53

Figure 15.	Comparison of the best fit 0.5 mm Bi in Sn experimental results and published Bi in Sn liquid diffusion studies.	54
Figure 16.	Comparison of the best fit 0.5-mm Zn in Sn experimental results and published Bi in Sn liquid diffusion studies.	56
Figure 17.	The best curve fit for the thin-film diffusion of Bi in Sn in a 1.6 mm diameter capillary after 6 hours at 973 K.	57
Figure 18.	The best curve fit for the thin-film diffusion of Bi in Sn in a 0.8 mm diameter capillary after 3 hours at 973 K.	58
Figure 19.	The best curve fit for the thin-film diffusion of Bi in Sn in a 0.5 mm diameter capillary after 3 hours at 973 K.	59
Figure 20.	The best curve fit for the thin-film diffusion of Zn in Sn in a 1.6 mm diameter capillary after 3 hours at 873 K.	61
Figure 21.	The best curve fit for the thin-film diffusion of Zn in Sn in a 0.5 mm diameter capillary after 3 hours at 873 K.	61
Figure 22.	The apparent diffusion coefficient for diffusion of Bi in Sn as defined by the scaling and numerical analyses of Garandet et al. as function of the capillary diameter, compared to results obtained in this study at 873 K.	62
Figure 23.	The apparent diffusion coefficient on Bi in Sn as defined by the scaling and numerical analyses of Garandet et al. as function of the capillary diameter, compared to results obtained in this study at 973 K.	63
Figure 24.	Kinematic viscosity versus temperature for liquid Tin.	80
Figure 25.	Density versus temperature for liquid Tin.	81

Figure 26. Bismuth in Tin Binary Phase Diagram – Atomic Percent Bismuth versus Temperature. 84

Figure 27. Tin in Zinc Binary Phase Diagram – Atomic Percent Tin versus Temperature. 85

LIST OF TABLES

Table 1.	Bi in Sn – Summary of interdiffusion studies from literature.....	30
Table 2.	Zn in Sn – Summary of interdiffusion studies from literature.....	33
Table 3.	Liquid diffusion of Bi in Sn – 0.5 mm capillary diameter dataset.....	45
Table 4.	Liquid diffusion of Bi in Sn – 0.8 mm capillary diameter dataset.....	46
Table 5.	Liquid diffusion of Bi in Sn – 1.6 mm capillary diameter dataset.....	47
Table 6.	Liquid diffusion of Zn in Sn – 0.5 mm capillary diameter dataset.	48
Table 7.	Liquid diffusion of Zn in Sn – 1.6 mm capillary diameter dataset.	48
Table 8.	Liquid Diffusion of Bismuth in Tin - 0.5 mm Capillary Diameter.....	75
Table 9.	Liquid Diffusion of Bismuth in Tin - 0.8 mm Capillary Diameter.....	76
Table 10.	Liquid Diffusion of Bismuth in Tin – 1.6 mm Capillary Diameter	77
Table 11.	Liquid Diffusion of Zinc in Tin - 0.5 mm Capillary Diameter	78
Table 12.	Liquid Diffusion of Zinc in Tin – 1.6 mm Capillary Diameter	78
Table 13.	Select physical properties of Tin	79
Table 14.	Numerical values for kinematic viscosity as a function of temperature of liquid Tin	80
Table 15.	Numerical values for density as a function of temperature for liquid Tin....	81
Table 16.	Select physical properties of Bismuth.....	82
Table 17.	Select physical properties of Zinc	83

1 INTRODUCTION

Liquid metal diffusion is an important atomic transport phenomenon which influences the solidification and structure of cast materials including metals, polymers and ceramics. Several theories have been advanced which attempt to determine atomic transport within liquid metals, but a single theory which accurately predicts liquid diffusion remains elusive.

The development of theory in the past has been predicated on published data which is inherently flawed, a direct result of the experimental method employed. Recently, experiments conducted in microgravity have offered new insight into diffusion research, and have established a benchmark for terrestrial experimentation. In the absence of gravity, liquid metal is not susceptible to mass transport induced by buoyancy driven convection, which results from horizontal temperature gradients across a capillary during annealing. However, experiments conducted in microgravity are cost prohibitive, and are subject to other sources of error. ^[1]

In order to develop a single theory of liquid diffusion, accurate diffusion coefficients for liquid metal systems must be determined, and an effective experimental technique capable of producing accurate diffusion coefficients under 1-g conditions must be developed.

This research was conducted with the objectives of determining interdiffusion coefficients for Bismuth (Bi) and Zinc (Zn) in liquid Tin (Sn), and to study the effect

capillary diameter has on the diffusion coefficient using the thin-film long capillary experimental method. It is hypothesized that by decreasing the capillary diameter, the horizontal temperature gradients which arise during annealing will be minimized and that the corresponding buoyancy driven mass transport will be suppressed, yielding lower values for the diffusion coefficient than those reported in literature.

The Bi-Sn and Zn-Sn systems were chosen for experimentation due to the relatively low melting temperatures of their constituents, their ease of handling and because of the availability of accurate liquid diffusion data for pure Sn which served as a reference for experimental findings.

2 LITERATURE REVIEW

2.1 Fick's Laws

Diffusion can be defined as a process of mass transport which results from random atomic or molecular motion in a system. The transfer of heat by conduction is analogous to this description, and in 1855, Adolph Fick quantified diffusion by utilizing the mathematical equation of heat conduction derived by Fourier in 1822. ^[2] The derivation of Fick's Laws has been summarized by Shewmon, and is described below. ^[3]

2.1.1 The Flux Equation – Fick's First Law

In inhomogeneous single phase alloys, matter flows in the direction of decreasing concentration. If the flux across a given plane is proportional to the concentration gradient across that plane and x is taken parallel to the concentration gradient of component 1, the flux of component 1 (J_1) at any time t is stated

$$J_1 = -D_1 \left[\frac{\partial c_1}{\partial x} \right]_t \quad (1)$$

where D_1 is the diffusion coefficient, and $\left[\frac{\partial c_1}{\partial x} \right]_t$ is the concentration gradient at time t .

This equation is Fick's first law and satisfies the empirical fact that the flux approaches zero as the specimen reaches equilibrium (homogeneous) and the concentration gradient approaches zero.

2.1.2 The Diffusion Equation – Fick's Second Law

If the concentration at a point is changing with time, Equation (1) is valid but must be modified. For a bar of unit cross-sectional area with the x axis along its center, the flux J_1 entering an element Δx can be related to the flux J_2 exiting (Figure 1) by the equation

$$J_1 = J_2 - \Delta x \left[\frac{\partial J}{\partial x} \right]. \quad (2)$$

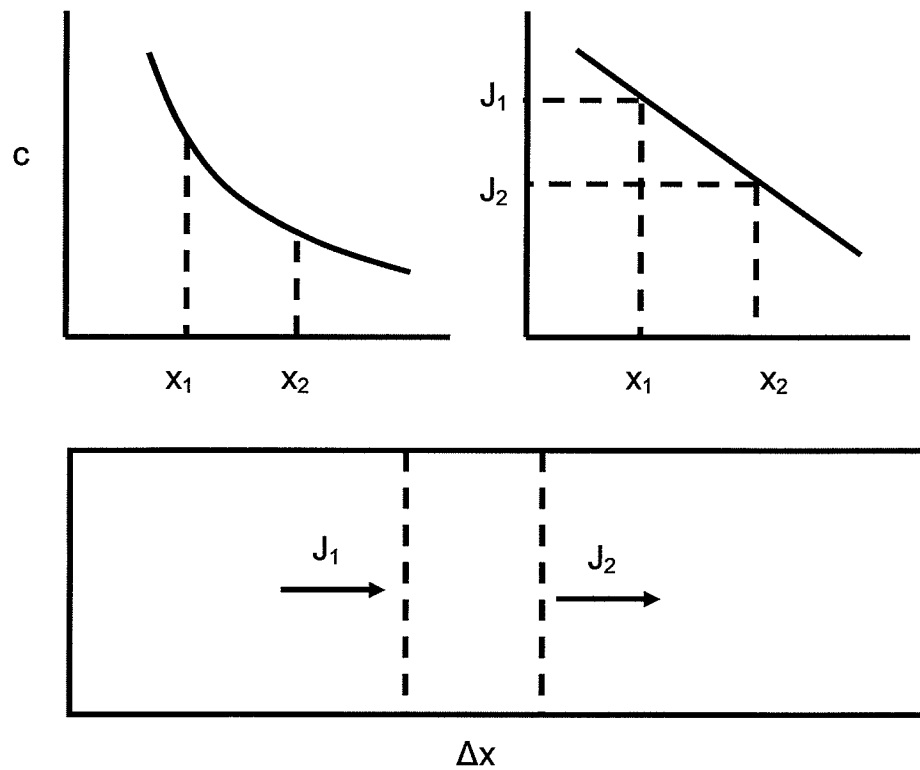


Figure 1. A graphical representation of the relationship between concentration, flux, and element of incremental distance.

Since the amount of material that entered the element in a unit time differs from that which exited, the concentration in the element has changed. For a volume $1 * \Delta x$, or the unit area times the thickness, the net increase in matter in the element can be expressed

$$J_1 - J_2 = \Delta x \left[\frac{\partial c}{\partial t} \right] = -\Delta x \left[\frac{\partial J}{\partial x} \right]. \quad (3)$$

Substitution of Equation (1) (which is valid even if concentration and concentration gradient at that point are changing with time) into Equation (3) yields Fick's second law of diffusion

$$\frac{\partial c}{\partial t} = \frac{\partial}{\partial x} \left[D \frac{\partial c}{\partial x} \right]. \quad (4)$$

2.2 The Diffusion Equation - Solutions

The following subsections develop the mathematical framework upon which diffusion research is based. By manipulating Fick's Second Law, the differential equation can be solved for a variety of conditions and the mathematics applied to experimental methodology. Common solutions referenced in literature are discussed to offer insight regarding the experimental techniques listed in *Section 2.4*.

2.2.1 Solution for Constant D

If the diffusion coefficient is assumed to be constant and not a function of position or concentration, Equation (4) can be simplified and rewritten

$$\frac{\partial c}{\partial t} = D \frac{\partial^2 c}{\partial x^2}. \quad (5)$$

Solutions for the concentration $c(x,t)$ as a function of position and time can be obtained by imposing various conditions on Equation (5).^[4]

2.2.1.1 The Thin-Film Solution

Imagine a semi-infinite bar of solute free material has plated to it a thin-film of solute with an initial concentration c_o . If the film of thickness b is annealed for a time t , the resulting concentration of solute along the bar is given by the equation

$$c(x,t) = \frac{bc_o}{\sqrt{\pi Dt}} e^{\left[\frac{-x^2}{4Dt}\right]} \quad (6)$$

in those regions for $\sqrt{Dt} > b$ (where x is the distance in either direction normal to the initial solute film). Equation (6) is a solution of the non-steady-state constant D diffusion equation (Equation (5)) which satisfies the boundary conditions

$$\text{for } |x| > 0, c \rightarrow 0 \text{ as } t \rightarrow \infty$$

$$\text{for } |x| = 0, c \rightarrow \infty \text{ as } t \rightarrow 0$$

where the total amount of solute remains constant as defined by Equation (7).

$$\int_0^{\infty} c(x,t) dx = bc_0 \quad (7)$$

For clarity, a graphical explanation of Equation (6) can be seen in Figure 2. The various curves (solutions for increasing values of t) demonstrate that although the solute concentration may travel a greater distance along the x axis with increasing time, the final concentration profile must adhere to Equation (7), meaning the total area under the curve must remain constant.

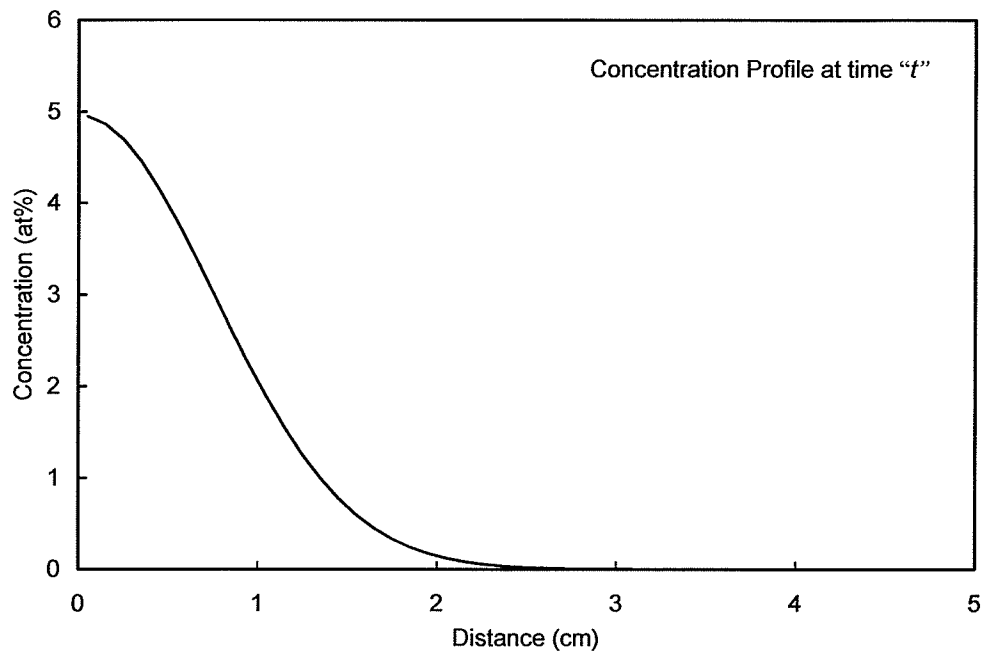
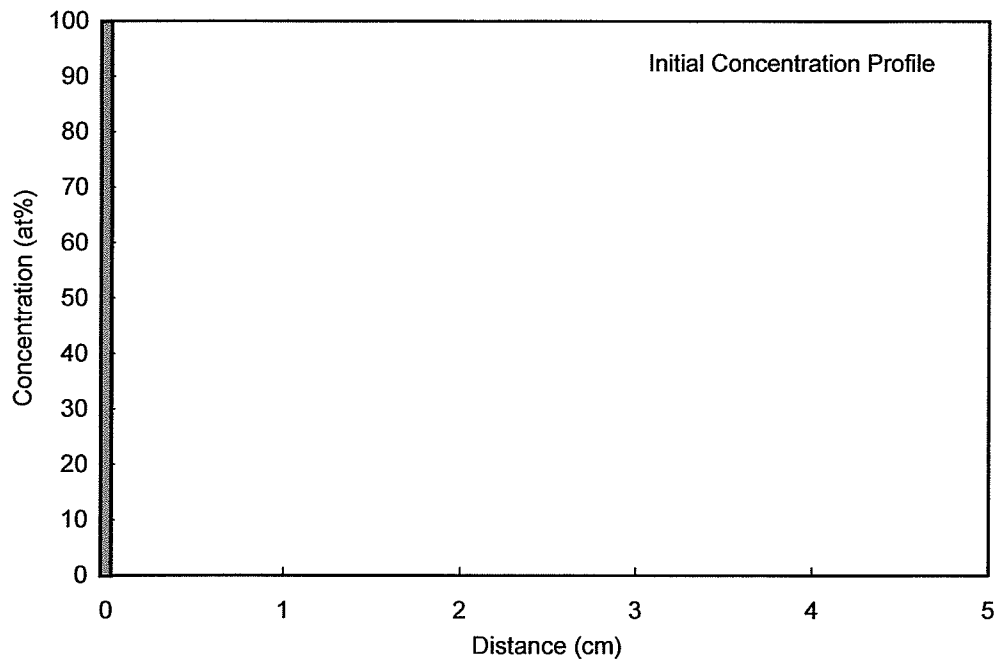


Figure 2. Concentration profiles before and after diffusion for the thin-film solution of the diffusion equation.

Although theoretically Equation (6) yields a solution for an infinite bar, in order to validate this expression experimentally, an approximation must be made. If an arbitrary minimum value for the concentration of 0.1% of c_0 is assigned, it is possible to specify a distance at which a bar of definite length can be assumed infinite.

$$0.001 \cdot c_0 = (bc_0) \int_{x'}^{\infty} c(x,t) dx \quad (8)$$

Solving Equation (8) for the distance x' , where bc_0 is the total quantity in the bar and the integrated term is the quantity beyond x' , the equation yields the solution for the length

$$x' = 4.6\sqrt{Dt} \quad (9)$$

As can be clearly seen from Equation (9), the assumption that a bar is “infinite” (for experimental purposes) is predicated on the value of the diffusion coefficient and the elapsed experimental time.

2.2.2 Solution for Variable D

If the diffusion coefficient does not remain constant, but varies along the concentration gradient as a function of position, Fick's second law must be written as

$$\frac{\partial c}{\partial t} = \frac{\partial}{\partial x} \left(D \frac{\partial c}{\partial x} \right) = \frac{\partial D}{\partial x} \frac{\partial c}{\partial x} + D \frac{\partial^2 c}{\partial x^2} \quad (10)$$

The solutions for this treatment of Fick's second law becomes difficult or impossible to solve analytically, but of common interest is the following solution for $D = D(c)$.^[5]

2.2.2.1 Boltzmann Transformation and the Matano Analysis

Boltzmann showed that for specific boundary conditions, if $D = D(c)$, Equation (10) can be transformed into an ordinary differential equation by introducing the variable $u = x/\sqrt{t}$. Using this definition of u ,

$$\frac{\partial c}{\partial t} = \frac{dc}{du} \frac{\partial u}{\partial t} = -\frac{1}{2} \frac{x}{t^{3/2}} \frac{dc}{du} \quad (11)$$

and

$$\frac{\partial c}{\partial x} = \frac{dc}{du} \frac{\partial u}{\partial x} = -\frac{1}{t^{1/2}} \frac{dc}{du} \quad (12)$$

Substitution of Equations (11) and (12) into Equation (10) yields

$$-\frac{x}{2t^{3/2}} \frac{dc}{du} = \frac{\partial}{\partial x} \left(\frac{D}{\sqrt{t}} \frac{dc}{du} \right) = \frac{1}{t} \frac{d}{du} \left(D \frac{dc}{du} \right) \quad (13)$$

or

$$-\frac{u}{2} \frac{dc}{du} = \frac{d}{du} \left(D \frac{dc}{du} \right) \quad (14)$$

Matano devised the first method to determine $D(c)$ by using the Boltzmann transformation, in which two infinite bars joined at an interface (forming diffusion couple) are subject to the following boundary conditions.

$$c = c_0 \quad \text{for } x < 0, \text{ at } t = 0$$

$$c = 0 \quad \text{for } x > 0, \text{ at } t = 0$$

Because the time $t=0$ and the interface position $x=0$ are excluded, the original concentration is not a function of position, and can be written in terms of u as

$$c = c_0 \quad \text{at } u = -\infty$$

$$c = 0 \quad \text{at } u = \infty$$

and when Equation 14 is integrated between $c=0$ and $c=c'$ (where c' is defined as the concentration $0 < c' < c_0$), it becomes

$$-\frac{1}{2} \int_{c=0}^{c=c'} u dc = \left[D \frac{dc}{du} \right]_{c=0}^{c=c'} \quad (15)$$

If a concentration versus distance profile $c(x)$ is produced at a fixed time, substituting for u obtains

$$-\frac{1}{2} \int_0^{c'} x dc = Dt \left[\frac{dc}{dx} \right]_{c=0}^{c=c'} = Dt \left(\frac{dc}{dx} \right)_{c=c'} \quad (16)$$

This infinite system has the condition $dc/dx=0$ at $c=0$, and similarly because $dc/dx=0$ at $c=c_0$, the condition is imposed that $\int_0^{c_0} xdc=0$. With this definition, Equation (16) defines the plane at which $x=0$, and the diffusion coefficient for any concentration c' can be obtained using Equation (17) as defined below.

$$D(c') = -\frac{1}{2} \left(\frac{dx}{dc} \right)_{c'} \int_0^{c_0} xdc \quad (17)$$

To use Equation (17), the Matano Interface must first be determined followed by the slope dx/dc at the desired position, as shown in Figure 3.

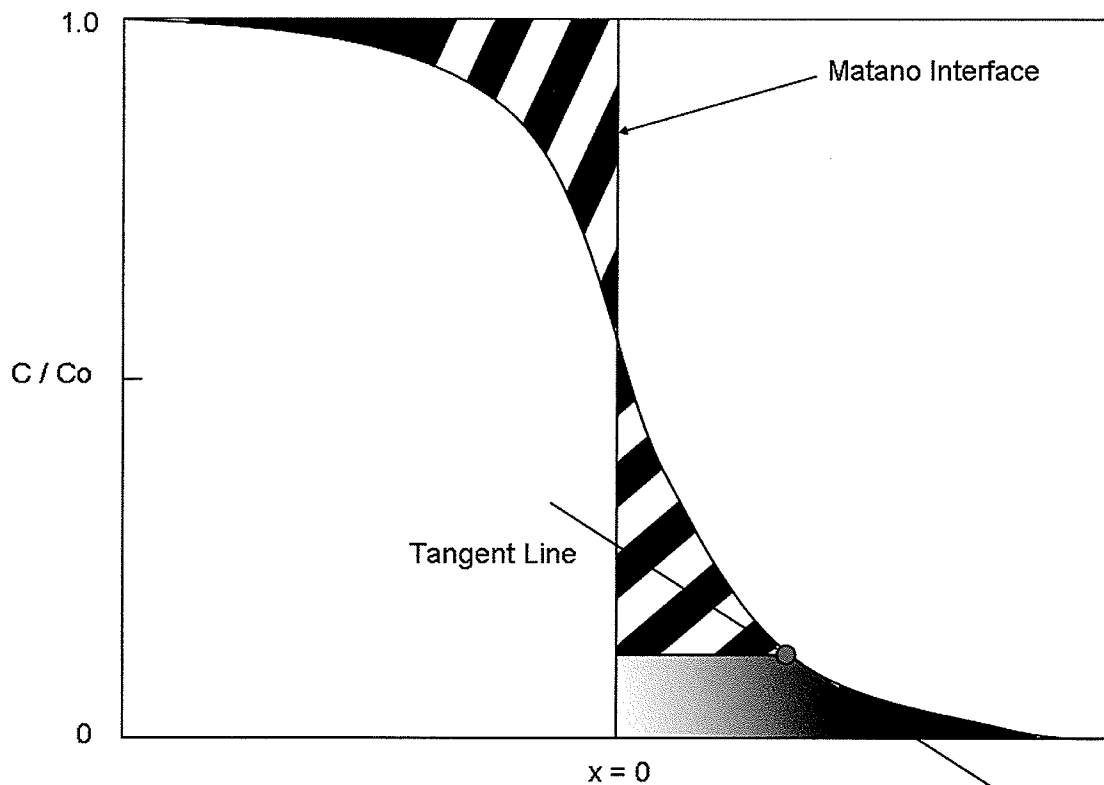


Figure 3. An example of a Boltzmann-Matano concentration versus distance diffusion plot.

2.2.3 Finite Difference Numerical Solution

In finite difference numerical solution ^[6], Fick's second law for a variable diffusion coefficient D is written

$$\frac{\partial c}{\partial t} = \frac{\partial}{\partial x} \left(D \frac{\partial c}{\partial x} \right) = \frac{\partial D}{\partial x} \frac{\partial c}{\partial x} + D \frac{\partial^2 c}{\partial x^2} = \frac{\partial D}{\partial c} \left(\frac{\partial c}{\partial x} \right)^2 + D \frac{\partial^2 c}{\partial x^2} \quad (18)$$

where D varies with concentration following the parabolic relationship given below, where the values of K_i are constant.

$$D = K_1 C^2 + K_2 C + K_3 \quad (19)$$

$$\frac{\partial D}{\partial c} = 2K_1 C + K_2 \quad (20)$$

Equation (19), when written in finite difference format appears as Equation (21), which can be solved using spreadsheet software such as MS Excel.

$$\frac{c_{i,t} - c_{i,t-1}}{\Delta t} = \left[\frac{\left(2K_1 c_{i-1,t-1} + K_2 \right) \left(\frac{c_{i+1,t-1} - c_{i-1,t-1}}{2} \right)^2}{\Delta x^2} \right] + \left[\left(K_1 D^2 + K_2 D + K_3 \right) \left(\frac{c_{i+1,t-1} - 2c_{i,t-1} + c_{i-1,t-1}}{\Delta x^2} \right) \right] \quad (21)$$

2.3 Liquid Metal Diffusion Theory

In this section, several theories of liquid diffusion in metals are presented. The defining equations of the models are listed for reference only, for in this thesis all data has been expressed in terms of the Arrhenius relationship. Although it has been proven that a “hole” theory for liquid metals is improbable ^[7], the Arrhenius relationship is a well established and convenient format for the presentation of diffusion data.

2.3.1 Hole Theory

The “hole” theory for liquid metals is analogous to the vacancy theory for diffusion in solids ^[8], where atoms are in constant motion (oscillating about their equilibrium positions), and migrate in a stepwise manner through vacant sites within the crystal/liquid. In the theory, diffusion is controlled by a thermally activated process following the Arrhenius relationship ^[9], defined

$$D = D_o e^{\left(\frac{-Q_o}{RT}\right)}, \quad (22)$$

where Q_o is the activation energy, D_o the frequency factor, R the universal gas constant, D the diffusion coefficient, and T the temperature. Taking the natural logarithm of Equation (22) produces the linear relationship summarized below, from which the activation energy and frequency factor can be easily calculated using linear regression.

$$\ln(D) = \ln(D_o) + \left[\frac{-Q}{RT}\right] = E + FT^{-1} \quad (23)$$

$$Q = -RF \quad (24)$$

$$D_o = \exp(E) \quad (25)$$

2.3.2 Fluctuation Theory

Swalin ^[10] proposed in "fluctuation" theory that liquid diffusion occurs via the movement of atoms through small and variable distances as a result of local density fluctuations. In the theory, transport occurs by the cooperative motion of five atom groups, but there is no specific activation energy because there is little difference between the atoms in participating groups and those that are not. The diffusion equation is given by

$$D = \frac{1}{6} \overline{j^2} \Gamma, \quad (26)$$

where $\overline{j^2}$ is the mean square value of a fluctuation distance which is considerably less than the atomic diameter and Γ is the fluctuation frequency. The mean square fluctuation distance is given by:

$$\overline{j^2} = \frac{3kT}{4\kappa}, \quad (27)$$

where k is Boltzmann's constant and κ is a force constant obtained from compressibility data. For this model, the diffusivity has a T^2 dependence and is given by

$$D = \frac{Zk^2T^2}{8h\kappa} \quad (28)$$

where Z is the coordination number and h is Planck's constant.

Also of note, Swalin and Leak ^[11] put forth a modified version of fluctuation theory, which will not be discussed in detail but is listed for reference.

2.3.3 *Vibrational and Molecular Friction Models*

In Nachtrieb's ^[12] vibrational model, liquid diffusion has a linear dependence on temperature as given by

$$D = \frac{k^2 \theta_D T}{h \kappa}, \quad (29)$$

where θ_D is the Debye temperature and κ is the force constant determined from compressibility data.

In addition, Nachtrieb with Rice ^[13] proposed a molecular friction model in which the diffusivity is given by

$$D = \frac{kT}{\zeta}, \quad (30)$$

where ζ is a frictional coefficient obtained from complex relationships involving pair correlation functions.

2.3.4 *Viscosity Based Theories*

Several models for liquid diffusion that involve the viscosity of the liquid η , have been developed and include the equations of Stokes-Einstein, Sutherland and Eyring. The diffusion coefficient for these models is given by ^[14]

$$D = \frac{kT}{B_I r \eta}, \quad (31)$$

where r is the atom radius and B_I is a constant that varies from about 2 to 6π depending upon the particular model.

Dullien ^[15] developed a viscosity-based model with the diffusivity given by

$$D = \frac{\delta^2 RT}{2\eta V}, \quad (32)$$

where δ is the average momentum transfer distance and V is the molar volume.

In Walls and Uptegrove's ^[16] theory, the diffusion coefficient is given by

$$D = \frac{kT\gamma^{-1/3}}{2\pi hb(2b+1)} \left(\frac{V}{N_0}\right)^{2/3} \exp\left(\frac{\Delta S^*}{R}\right) \exp\left(\frac{-\Delta H^*}{RT}\right), \quad (33)$$

where γ is a constant with a value of 4/3, b is the ratio of the effective atomic radius to the interatomic distance, V is the molar volume, N_0 is Avogadro's number, and ΔS^* and ΔH^* are the entropy and enthalpy for viscosity.

Hines and Walls ^[17] related the diffusion process to atomic arrangements as described by the radial distribution function. In their theory, it is assumed that the liquid vibrational frequency is linearly dependent upon temperature, as stated

$$D = \frac{1}{6} f^2 \nu_s \{\exp[-\Delta H_F / RT_m]\}^{1/3} \frac{T}{T_m} \frac{\eta_m}{\eta} \frac{(12-Z)}{2}, \quad (34)$$

where f is the fluctuation distance, ν_s is the vibrational frequency of the solid at the melting temperature, ΔH_F is the latent heat of solidification, T_m is the melting temperature, η_m is the viscosity of the liquid metal at the melting temperature, η is the viscosity of the liquid at temperature T , and Z is the coordination number.

2.3.5 Sphere Models

If it is assumed that a liquid is an agglomeration of hard spheres, and each sphere has a coordination number of 12 (most dense packing), D is defined by Peter et al. [18] as

$$D = 5.17 \times 10^{-16} \nu (\Delta V)^2 \left(\frac{Q}{RT} \right)^{5/2} \exp(-Q/RT) \quad (35)$$

where ν is the Debye frequency of the liquid (taken as 90% that of the solid) and ΔV is the volume change upon melting.

From the kinetic theory of gases, a model for liquid diffusion has been derived in which atoms are treated as rigid elastic spheres. Using Enskog's solution of the Boltzmann Transport Equation [19], the liquid diffusion coefficient is given by [20]

$$D_{ENS} = \frac{3}{8} \frac{\nu}{\sigma^2} \left(\frac{kT}{\pi M} \right)^{1/2} \left(\frac{1}{C_0^{(2)}} \right), \quad (36)$$

where ν is the volume occupied per sphere, σ is its diameter, M is its mass, and $C_0^{(2)}$ is the equilibrium pair correlation function which has a value of unity for uncorrelated fluids. In this theory, the atomic diameter σ , is given by

$$\sigma = 1.126 \sigma_m \{10.112(T/T_m)^{1/2}\} \quad (37)$$

where σ_m is the atomic diameter at the melting temperature, T_m .

As a corollary, a corrective factor which scales Equation (36) has been proposed in response to the "cage effect", whereby any particular sphere's motion is prevented by a cage of neighboring spheres. [20, 21]

Finally, Cohen and Turnbull ^[22] using a rigid sphere model and the “free volume” concept derived a value for the diffusion coefficient given by

$$D = g\sigma^* \left(\frac{3kT}{M} \right)^{1/2} \exp\left(\frac{-\gamma V^*}{V_f} \right), \quad (38)$$

where g is a geometric factor, σ^* is taken as equal to the atomic diameter, M is the atomic mass, γ is a constant with a value $0.5 < \gamma < 1.0$, V^* is the critical free volume for atomic motion per cell, and V_f is the average free volume per cell.

2.4 Liquid Metal Diffusion Experimental Techniques

Several experimental techniques have been devised to determine the diffusion coefficients of liquid metals; these include but are not limited to the long capillary, the capillary reservoir, and shear cell methods. The three techniques listed are the most common found in literature and will be discussed further.

2.4.1 The Long Capillary Method

The long capillary method, as the name implies, uses a long cylindrical capillary to contain a liquid metal diffusion couple. The capillary is created by boring a hole into the inert material (generally made of ceramic or graphite), leaving it sealed at one end. The concentration and relative amount of solute and solvent vary according to the desired type of diffusion experiment, as the technique can be used for a variety of mathematical analyses. Once filled, the end of the capillary is sealed and is immediately heated in a furnace to the desired experimental temperature. After a specified period of time has elapsed, the specimen is removed from the furnace and allowed to cool rapidly.

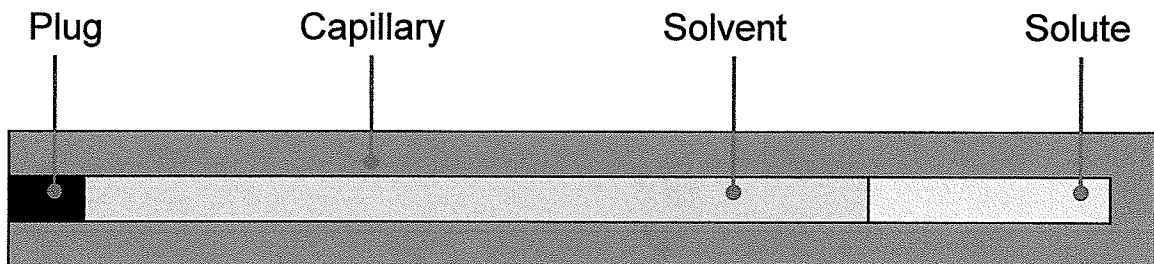


Figure 4. A diagram of a long capillary.

2.4.2 The Capillary Reservoir Method

In the capillary reservoir technique [23], a capillary (sealed at one end) is filled with the solute metal or an alloy of the solute and solvent of known concentration. The capillary is then immersed in the reservoir, which consists of a bath of solvent metal in a large crucible. The immersed capillary is held at a constant temperature for a measured time, and is then removed from the bath and allowed to cool. The diffusion coefficient is then determined from the material in the capillary. The capillary is placed in the bath in the vertical position with the more dense material placed at the bottom, while a vertically increasing temperature gradient is maintained (in an attempt to suppress buoyancy driven convection). If the diffusion coefficient is assumed constant, Fick's second law is subjected to the initial condition

$$c(x,0) = c_0 \text{ for } 0 < x < L$$

with the following boundary conditions

$$\frac{\partial c(0,t)}{\partial x} = 0 \text{ for } t > 0, \quad c(L,t) = c_0 \text{ for } t > 0$$

which yields a solution for the concentration profile $c(x,t)$. The concentration profile is then integrated over the length of the capillary L to produce a solution for the average concentration in the capillary $\bar{c}(t)$ for the measured time.

$$\bar{c}(t) = \frac{8}{\pi^2} \sum_{n=0}^{\infty} \frac{c_0}{(2n+1)^2} e^{\left[-\pi^2(2n+1)^2 \frac{Dt}{4L^2}\right]} \quad (39)$$

Equation (39) can then be solved to produce the constant diffusion coefficient.

$$D = \frac{4L^2}{\pi^2 t} \ln \frac{\pi^2 \bar{c}}{8 c_0} \quad (40)$$

2.4.3 *The Shear Cell Method*

The shear cell technique is a modified version of the long capillary method. Within a shear cell, a long capillary is divided into several sections which can be isolated during experimentation. Generally, several circular disks (forming a long cylinder) share a common capillary of constant diameter. Each disk rotates about a fixed axis, which allows the individual capillary sections to be misaligned during heating, aligned for the duration of the diffusion experiment, and then misaligned during the cooling stage. It is the intent of the experimental technique to minimize the effect of solute redistribution on the diffusion coefficient, which may occur during solidification of the capillary.

Following experimentation, the individual sections are chemically analyzed and the diffusion coefficient is determined from the resulting concentration versus distance profile. The shear cell technique can be used to perform both thin-film and Boltzmann-Matano type experiments, and offers precise control over the location of the initial diffusion couples interface. Figure 5 illustrates a basic shear cell, and the accompanying mechanism.

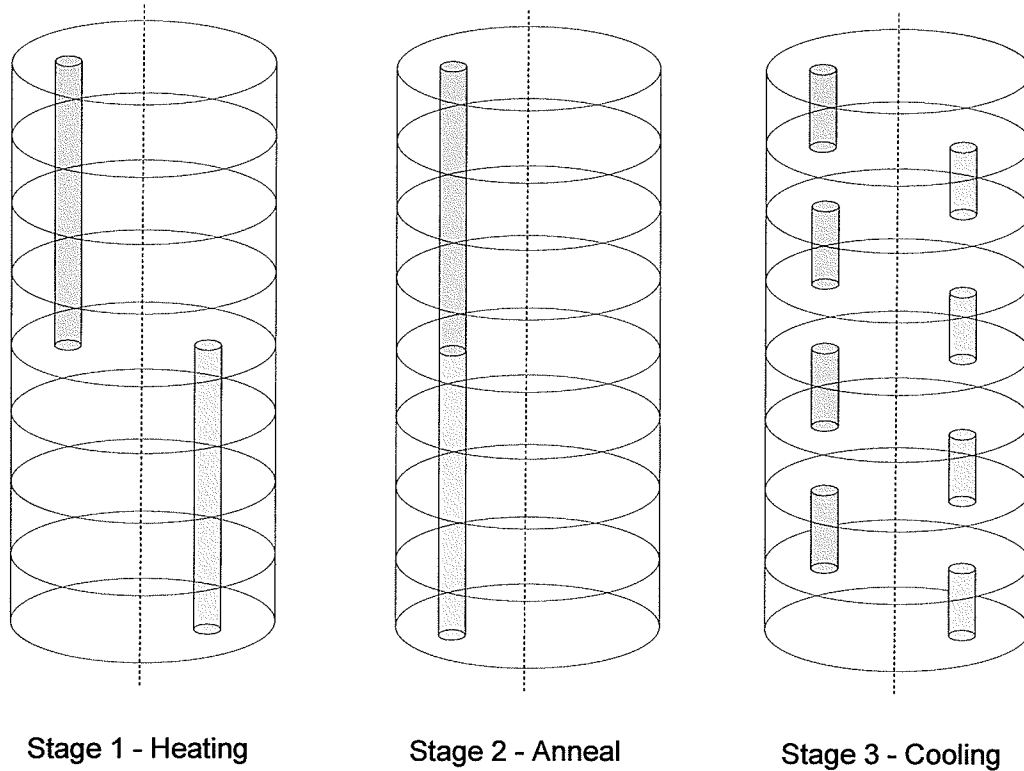


Figure 5. Schematic of a shear cell apparatus, showing the stages of shear: initial, aligned, and final position.

2.5 The Effect of Capillary Diameter on the Diffusion Coefficient

Under terrestrial conditions (1-g), diffusion coefficients obtained using the long capillary method may be influenced by convective processes, which result from local density differences within the liquid. Density differences, which arise as consequence of either a temperature gradient or a concentration gradient, can be suppressed during experimentation by orientating the capillary in the vertical direction. This was proven by Verhoeven ^[24], by manipulation of the Navier-Stokes equation for an incompressible fluid of constant viscosity within a gravitational field. The Navier-Stokes equation is given as

$$\frac{\partial V}{\partial t} + (V \cdot \Delta V) = -\frac{\nabla P}{\rho} + \nu \nabla^2 V - g \bar{k} \quad (41)$$

where V is the velocity, t the time, ρ the density, P the pressure, g the gravitational acceleration, ν the kinematic viscosity, and \bar{k} a unit vector in the vertical direction. If the liquid remains motionless during experimentation ($v = 0$), Equation (41) becomes

$$\frac{\nabla P}{\rho} + g \bar{k} = 0 \quad (42)$$

and the density can then be isolated by taking the curl of Equation (42)

$$\nabla \rho \times g \bar{k} = 0 \quad (43)$$

If the density variation within a binary solution is approximated by

$$\rho = \rho_0 [1 - \alpha(T - T_0) - \alpha'(C - C_0)] \quad (44)$$

where α is the thermal expansion coefficient, α' is the solute expansion coefficient, T the temperature and C the solute concentration, when combining Equations (44) and (43) a criteria is produced (Equation (45)) which shows that both the temperature and

concentration gradients must be oriented vertically to ensure a motionless fluid during experimentation.

$$\alpha \nabla T \times \bar{g} + \alpha' \nabla C \times \bar{g} = 0 \quad (45)$$

Verhoeven further classified the free convection produced by temperature and concentration gradients as “threshold convection” for vertical density gradients and “thresholdless convection” for horizontal density gradients. In his paper, it is stated that for a capillary in the vertical position, threshold convection may be suppressed by applying a positive stabilizing temperature gradient in the vertical direction and placing the heavier solute or solvent at the bottom of the capillary, but thresholdless convection may still arise due to lateral temperature variation. In his conclusion, an optimum capillary diameter of 1-mm to 2-mm is recommended to suppress both threshold and thresholdless convection, but is not discussed in detail. A more recent analysis has been conducted by Garandet et al. [25] which addresses the convection associated with a temperature differential across the capillary walls.

A temperature differential across the capillary walls is a direct result of the apparatus used to conduct liquid diffusion experiments. At elevated temperatures, a thermal gradient will be produced within the furnace due to the temperature differential between the chamber and the furnace surroundings (usually room temperature). Even with heavily insulated furnaces, extremely small temperature gradients can have a pronounced effect on the measured diffusion coefficient. Garandet et al. state that the convective

mass transfer will scale with the product of the Grashof and Schmidt numbers, defined by Equation (46)

$$Gr = \frac{\beta_T g_0 \Delta T_H H^3}{\nu^2} \quad (46)$$

where β_T is the thermal expansion coefficient, g_0 the gravity level, ν the kinematic viscosity, H the lateral dimension of the capillary, ΔT_H a measure of the horizontal temperature difference, and D the diffusion coefficient. They apply two distinct methods of analysis to this problem, including a scaling analysis and a numerical simulation which utilizes finite element analysis. The result of this effort yields an apparent diffusion coefficient D^* , that specifies the error within the diffusion coefficient in terms of the best known value of the diffusion coefficient D , taken to be the experimental value produced in microgravity (if available).

$$D^* = D(1 + R) \quad (47)$$

$$R = \frac{1}{4} H^2 \frac{W^2}{D^2} \quad (48)$$

In Equations (47) and (48), R represents the ratio of the convective and diffusive mass transfer coefficients and W the vertical component of the velocity vector. For the scaling R is defined as $R \approx (GrSc)^2 / 1500$, and similarly, for numerical analyses R is defined as $R = (GrSc)^2 / 4050$. In combining Equations (47) and (48), it is possible to isolate the effect of controllable experimental parameters, specifically capillary diameter. Figure 6 illustrates the apparatus, the capillary diameter, the orientation of the capillary in

reference to the gravity vector, and the direction of the temperature gradient with respect to the vertical axis of the cylindrical furnace.

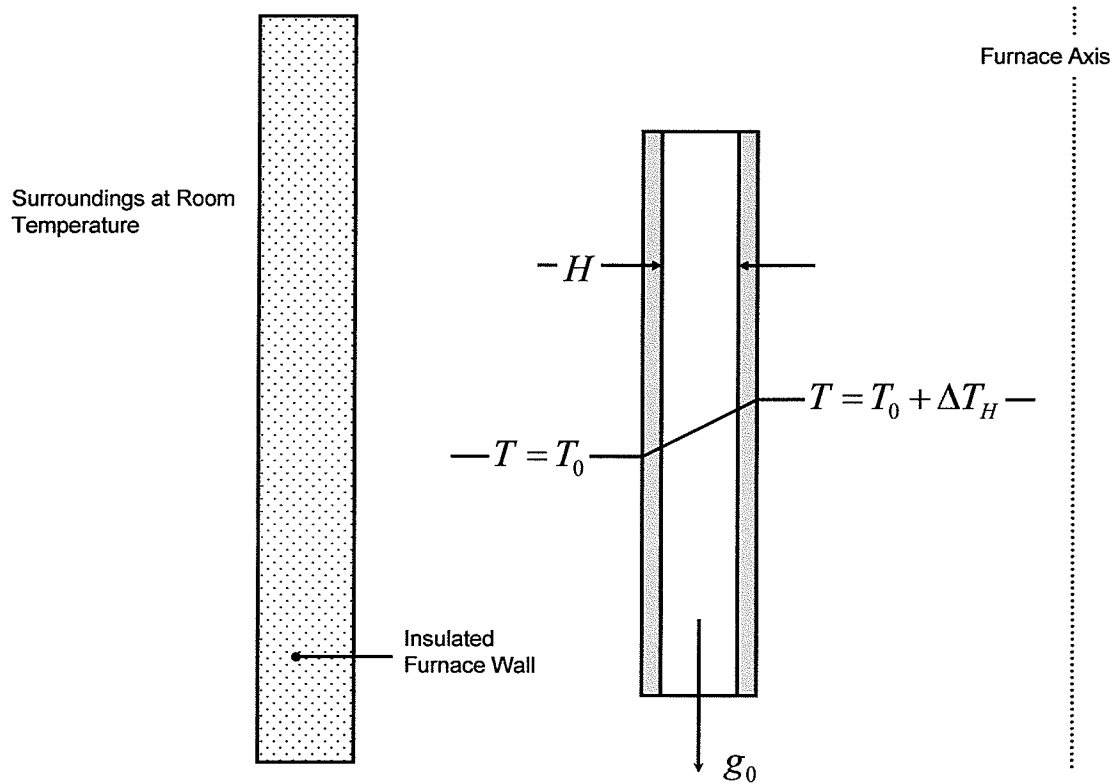


Figure 6. A long capillary liquid diffusion specimen orientated vertically within a furnace, subjected to a horizontal temperature gradient.

2.6 Diffusion Investigations from Literature

2.6.1 Solvent Self Diffusion of Liquid Tin

Figure 7 presents a summary of several solvent self-diffusion studies of Sn, which served as a source of reference and comparison during thesis research. The dataset, compiled by Cahoon et al. [26], has been analyzed and curve fit to produce the best fit parameters for solvent self diffusion of Sn of $Q = 12.10 \pm 0.37$ kJ/mole and $D_0 = 3.49 \pm 0.22 \times 10^{-8}$ m²/s.

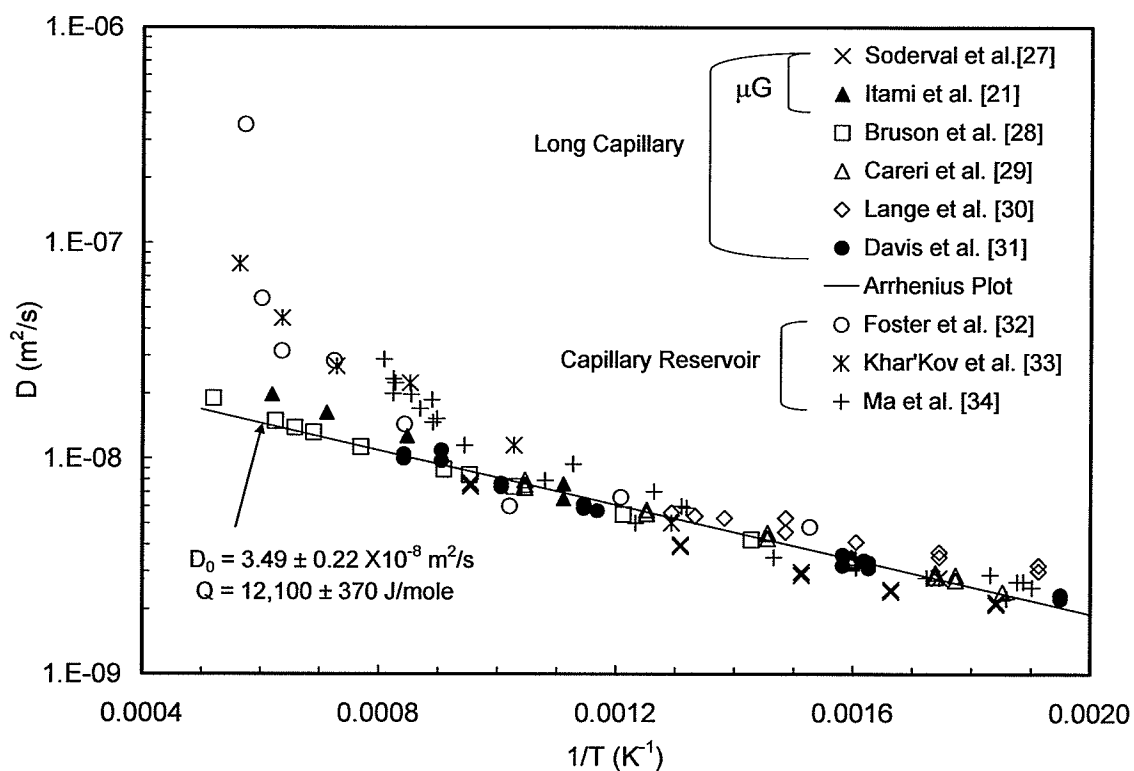


Figure 7. Arrhenius plot for the solvent self-diffusion of Sn.

2.6.2 Bismuth in Tin Interdiffusion

In Figure 8, the interdiffusion values for several Bi in Sn investigations are presented. [35, 36, 37, 38, 39] In Table 1, a summary of the data used in the creation of this figure is listed by author. Also included in the table is the experimental technique, acceleration acting on the experiment, and capillary diameter specific to each study.

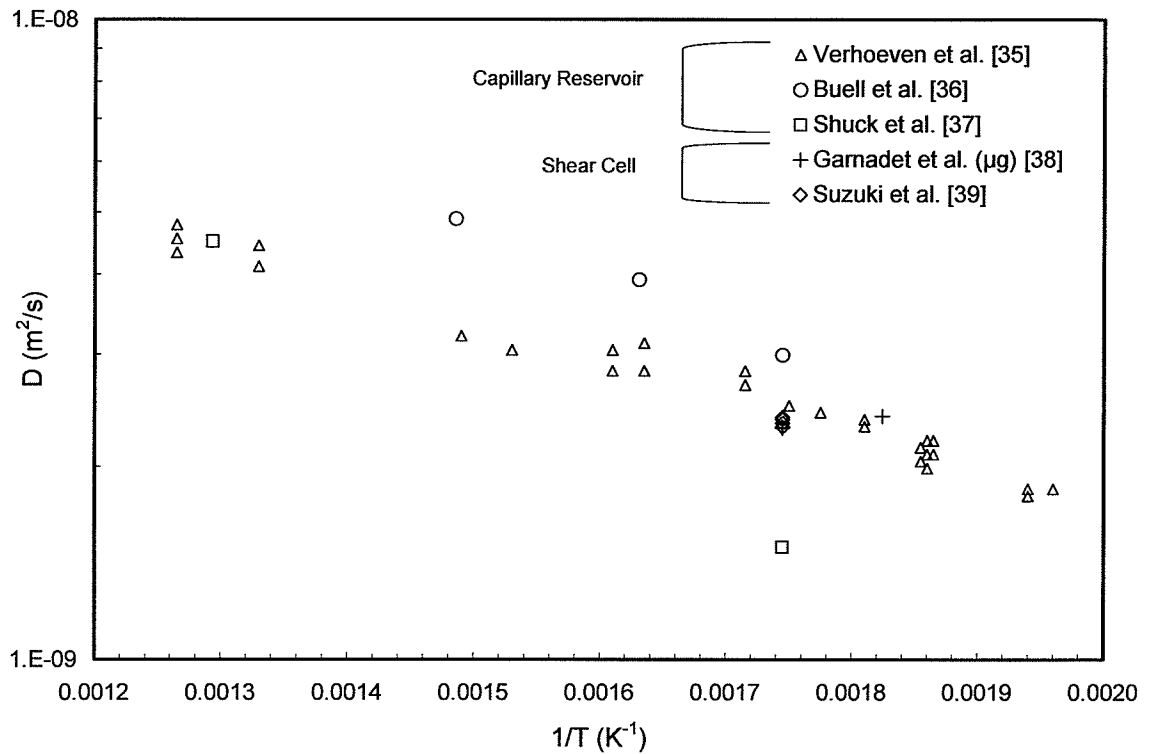


Figure 8. Bi in Sn – Summary of interdiffusion studies from literature.

Table 1. Bi in Sn – Summary of interdiffusion studies from literature*Verhoeven et al.* ^[35]

Temperature (K)	Experimental Technique	Acceleration	Capillary Diameter	Diffusion Coefficient (m ² /s x10 ⁹)
791	Capillary Reservoir	1 - g	1 - mm	4.77
791	Capillary Reservoir	1 - g	1 - mm	4.54
791	Capillary Reservoir	1 - g	1 - mm	4.32
752	Capillary Reservoir	1 - g	1 - mm	4.43
752	Capillary Reservoir	1 - g	1 - mm	4.11
671	Capillary Reservoir	1 - g	1 - mm	3.20
654	Capillary Reservoir	1 - g	1 - mm	3.04
621	Capillary Reservoir	1 - g	1 - mm	3.04
621	Capillary Reservoir	1 - g	1 - mm	2.82
612	Capillary Reservoir	1 - g	1 - mm	2.82
612	Capillary Reservoir	1 - g	1 - mm	3.12
583	Capillary Reservoir	1 - g	1 - mm	2.82
583	Capillary Reservoir	1 - g	1 - mm	2.82
583	Capillary Reservoir	1 - g	1 - mm	2.82
583	Capillary Reservoir	1 - g	1 - mm	2.69
583	Capillary Reservoir	1 - g	1 - mm	2.69
583	Capillary Reservoir	1 - g	1 - mm	2.69
571	Capillary Reservoir	1 - g	1 - mm	2.49
563	Capillary Reservoir	1 - g	1 - mm	2.43
552	Capillary Reservoir	1 - g	1 - mm	2.37
552	Capillary Reservoir	1 - g	1 - mm	2.31
539	Capillary Reservoir	1 - g	1 - mm	2.14
539	Capillary Reservoir	1 - g	1 - mm	2.04
538	Capillary Reservoir	1 - g	1 - mm	2.20
538	Capillary Reservoir	1 - g	1 - mm	2.09
538	Capillary Reservoir	1 - g	1 - mm	1.99
536	Capillary Reservoir	1 - g	1 - mm	2.20
536	Capillary Reservoir	1 - g	1 - mm	2.09
515	Capillary Reservoir	1 - g	1 - mm	1.85
515	Capillary Reservoir	1 - g	1 - mm	1.80
510	Capillary Reservoir	1 - g	1 - mm	1.85

Buell – Shuck ^[36]

Temperature (K)	Experimental Technique	Acceleration	Capillary Diameter	Diffusion Coefficient (m ² /s x10 ⁹)
573	Capillary Reservoir	1 - g	1.5 - mm	2.99
613	Capillary Reservoir	1 - g	1.5 - mm	3.92
673	Capillary Reservoir	1 - g	1.5 - mm	4.88

Shuck – Stover ^[37]

Temperature (K)	Experimental Technique	Acceleration	Capillary Diameter	Diffusion Coefficient (m ² /s x10 ⁹)
573	Capillary Reservoir	1 - g	-	1.50
773	Capillary Reservoir	1 - g	-	4.50

Garnadet et al. ^[38]

Temperature (K)	Experimental Technique	Acceleration	Capillary Diameter	Diffusion Coefficient (m ² /s x10 ⁹)
548	Shear Cell	μg	1.5 - mm	2.40
573	Shear Cell	μg	1.5 - mm	2.30

Suzuki et al. ^[39]

Temperature (K)	Experimental Technique	Acceleration	Capillary Diameter	Diffusion Coefficient (m ² /s x10 ⁹)
573	Shear Cell	1 - g	-	2.34
573	Shear Cell	1 - g	-	2.37
573	Shear Cell	1 - g	-	2.39
573	Shear Cell	1 - g	-	2.31

2.6.3 Zinc in Tin Interdiffusion

In Figure 9, the interdiffusion values for several Zn in Sn investigations are presented. [40, 41, 26] In Table 2, a summary of the data used in the creation of the figure is listed by author. Also included in the table is the experimental technique, acceleration acting on the experiment, and capillary diameter specific to each study.

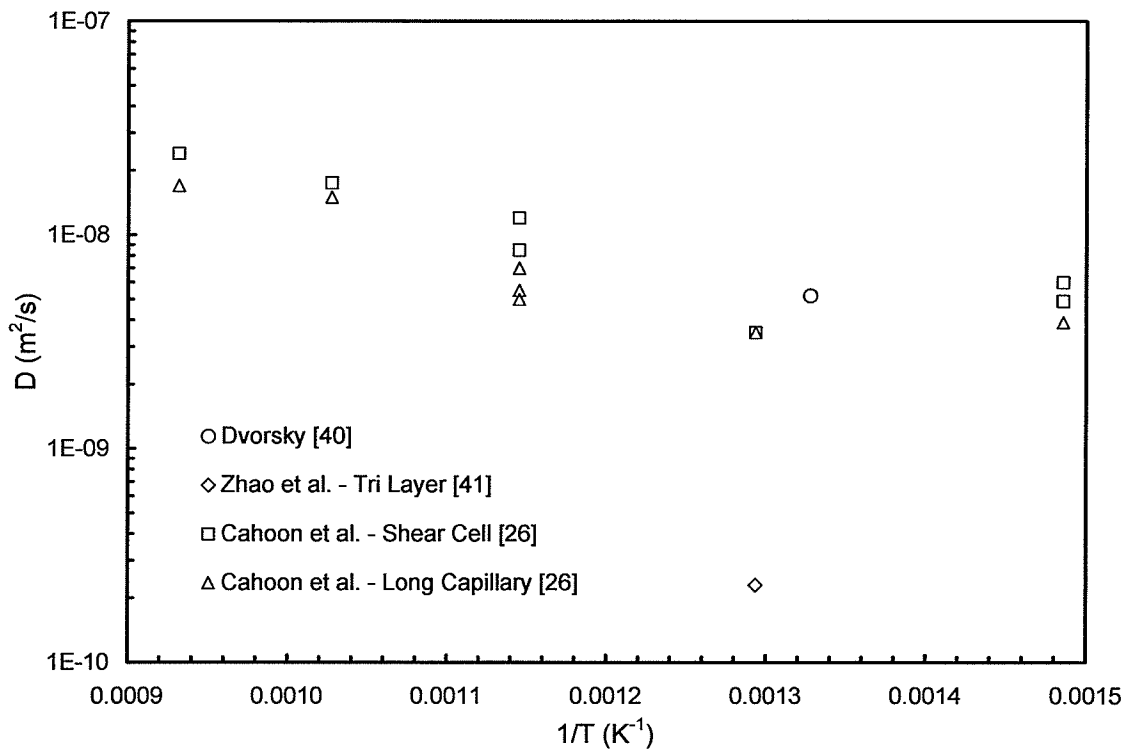


Figure 9. Zn in Sn – Summary of interdiffusion studies from literature.

Table 2. Zn in Sn – Summary of interdiffusion studies from literature*Dvorsky*^[40]

Temperature (K)	Experimental Technique	Acceleration	Capillary Diameter (mm)	Diffusion Coefficient (m ² /s x10 ⁹)
753	-	1-g	-	5.20

Zhao^[41]

Temperature (K)	Experimental Technique	Acceleration	Capillary Diameter (mm)	Diffusion Coefficient (m ² /s x10 ⁹)
773	-	1-g	-	0.23

Cahoon^[26]

Temperature (K)	Experimental Technique	Acceleration	Capillary Diameter (mm)	Diffusion Coefficient (m ² /s x10 ⁹)
673	Shear Cell	1-g	1.6	4.90
673	Shear Cell	1-g	1.6	6.00
773	Shear Cell	1-g	1.6	3.50
873	Shear Cell	1-g	1.6	8.50
873	Shear Cell	1-g	1.6	1.20
973	Shear Cell	1-g	1.6	1.75
1073	Shear Cell	1-g	1.6	2.40

Cahoon^[26]

Temperature (K)	Experimental Technique	Acceleration	Capillary Diameter (mm)	Diffusion Coefficient (m ² /s x10 ⁹)
673	Long Capillary	1-g	1.6	3.90
773	Long Capillary	1-g	1.6	3.50
873	Long Capillary	1-g	1.6	5.00
873	Long Capillary	1-g	1.6	5.50
873	Long Capillary	1-g	1.6	7.00
973	Long Capillary	1-g	1.6	15.00
1073	Long Capillary	1-g	1.6	17.00

3 EXPERIMENTAL METHODS

In this thesis, the long capillary solute disk technique was used to determine diffusion coefficients for the interdiffusion of both Bismuth and Zinc in Tin, and a modified Thin-film solution was used to calculate the resulting constant experimental diffusion coefficients.

3.1 Apparatus

3.1.1 Material Specifications

In this study, Sn was used as the solvent material and Bi or Zn as the solute. The Sn and Zn came in wire form at diameters of 1.6-mm, 1-mm, and 0.5-mm at $\geq 99.999\%$ purity, while the Bi came in powder form at 99.999-% purity. The graphite rod used for all experiments was 13-mm in diameter, and of 99.997-% purity. All materials were supplied by Alfa Aesar, MA, USA, or the Goodfellow Corporation, PA, USA.

3.1.2 Capillaries

Three sets of capillaries were created by drilling 1.6 mm, 0.8 mm, and 0.5 mm diameter holes into graphite rods 12.7 mm in diameter. Care was taken to ensure that the holes were drilled in the center of the rods and that the drill bit did not pass through the graphite, which left the hole sealed at the bottom end. The capillary length was set at 80 mm for the 1.6 mm diameter capillaries, and 50 mm for the 0.8 mm and 0.5 mm diameter capillaries.

3.1.3 *Vacuum Furnace*

The vacuum furnace consisted of a long vertical stainless steel tube welded closed at the bottom end (forming the chamber of the furnace), which was fitted with a brass cap at the top end of the furnace via a bolted flange connection. To ensure vacuum could be achieved, and similarly that the backfilled Argon atmosphere would remain contained during experimentation, the interface of the brass/stainless steel flange was fit with an o-ring and lubricated with vacuum grease. The furnace consisted of three stages of controlled heating zones surrounded by insulation, each capable of independent operation via an external controller. The temperature at the top of the furnace remained cool to the touch throughout experimentation by means of copper coils connected to a constantly flowing and pressurized chilled water supply. Passing through the center of the brass cap was a long stainless steel brass rod (sealed with two o-rings and vacuum grease) which was used to raise and lower the diffusion specimens from the cold to hot zone of the furnace. Also passing through the brass cap was a thermocouple, radially offset from the stainless steel rod, which was used to monitor the internal temperature of the vacuum furnace at the same elevation as the diffusion specimen. The furnace was evacuated using a rotary vacuum pump and backfilled with Argon from an external source. A series of valves were used to isolate the vacuum pump, the Argon source, and the internal atmosphere. In addition, the furnace was connected to a several pressure gauges which were used to monitor the chamber pressure. A schematic of the experimental apparatus is presented in Figure 10.

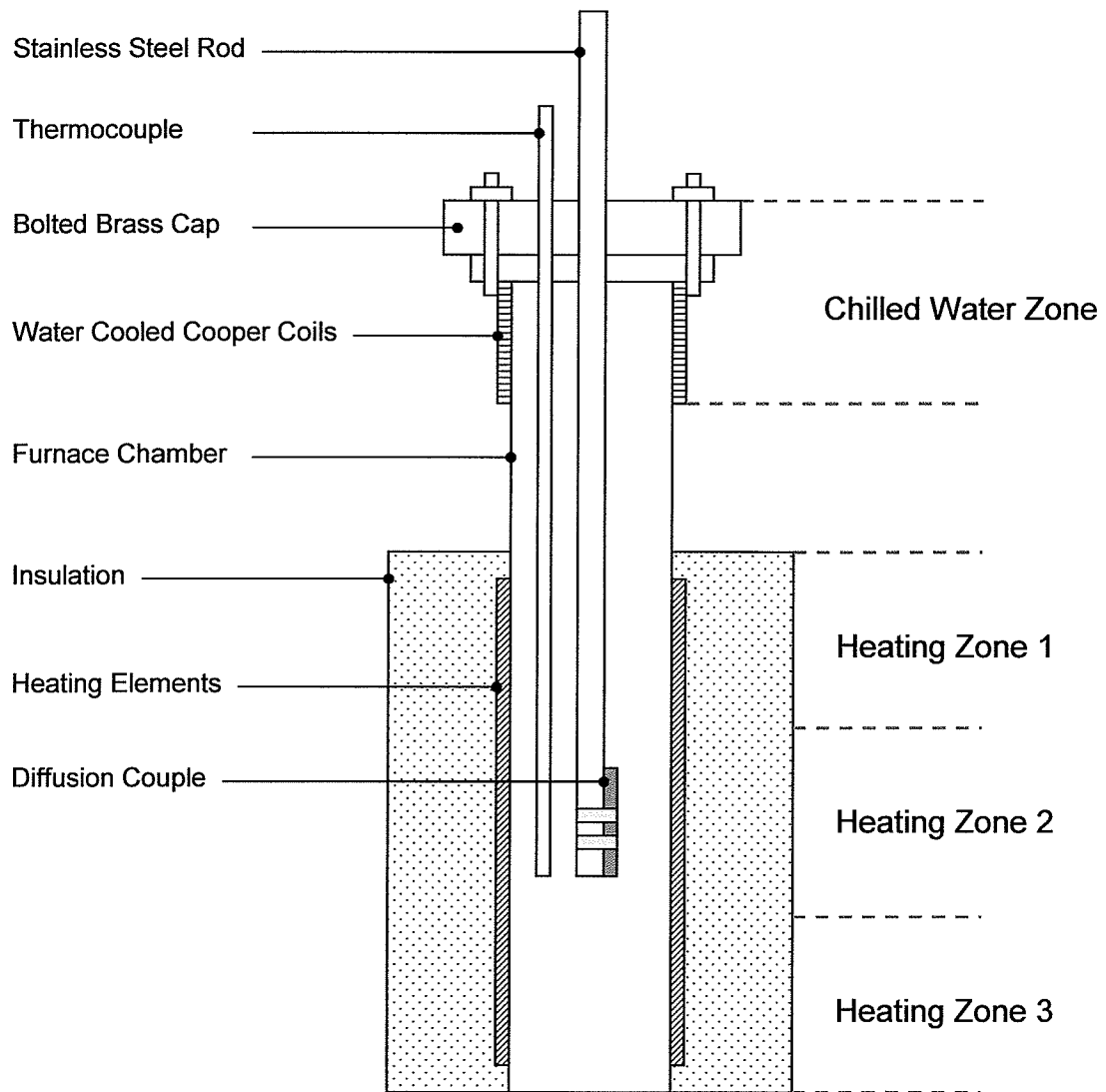


Figure 10. A schematic of the experimental apparatus utilized in this research.

3.1.4 Analytical Equipment

All samples were analyzed using a JEOL 9000 Scanning Electron Microscope (SEM) equipped with an Oxford Instruments Energy Dispersive Spectrometer (EDS). The EDS was used to perform quantitative chemical analysis via an INCA Energy software interface.

3.2 Procedure

3.2.1 *Diffusion Couple Preparation*

The diffusion couples were comprised of a graphite capillary, a disk of solute material (forming the thin-film of Bi or Zn), a long wire of solvent material (Sn), and a small graphite plug. All materials were thoroughly cleaned to remove oxides and oils several times during the sample preparation via sandpaper and/or an ultrasonic agitator. Thin cylindrical solute disks were created by sectioning graphite capillaries of cast solute of desired diameter with an IsoMet precision saw. Each individual solute disk was weighed and the mass recorded using an electronic scale accurate to four significant figures. A solute disk of material was then placed on either the top (for Zn) or the bottom (for Bi) of the capillary as defined by its liquid density relative to the density of liquid Sn. The remaining volume of the capillary was filled with solvent and sealed with a press fit graphite plug.

3.2.2 *Diffusion Anneal*

Once prepared, the diffusion couples were fastened to the stainless steel rod of the furnace apparatus with band clamps to ensure the samples remained vertical throughout the diffusion anneal. The furnace was cyclically evacuated three times to a pressure of 0.2-torr using a rotary pump, and backfilled with Argon gas to ensure an inert environment for experimentation. At all times during furnace ramp-up, the diffusion couples were in contact with the water-cooled brass cap of the furnace. Once the desired anneal temperature was reached, the diffusion couples were lowered from their ramp-up position into the heated zone of the furnace via the stainless steel rod. The exact

temperature at the sample was monitored using a thermocouple, and a slight temperature gradient (positive 2 – 3 K) in the vertical direction over the length of the heated zone of the furnace was maintained. At the end of the anneal period, the samples were immediately removed from the furnace and allowed to air cool (at all times remaining in the vertical position). Anneal temperatures ranging from 573 K to 1073 K were tested, with experimental durations varying from 2.5 h to 6 h (time was selected on the basis of sample length, anneal temperature, and the approximate range of the diffusion coefficient).

3.2.3 Sample Preparation

Upon cooling, the diffusion samples were carefully ground to produce a planar cross-section revealing the newly formed alloy rod. The samples, while still incased in graphite, were precut to lengths of 30 mm or less, at which point they were carefully extracted from their graphite casing. Following this, the samples were mounted in Lucite and polished to 0.25 μm with colloidal silica solution. At all stages of the process the samples were cleaned thoroughly using an ultrasonic agitator. Finally, the samples were prepared for SEM and chemical analysis using a combination of copper conducting tape and graphite paste.

3.2.4 Chemical Analysis

Once the integrity of the samples was verified using the SEM, quantitative chemical analysis was performed. The concentration distribution across the length of the diffusion capillaries was determined in 1 mm increments at 140x magnification using the SEM in

combination with the EDS. Beginning at the location of the thin-film, each data point was taken to be the average atomic concentration of the solute in the parent material over an area equal to the width of the capillary by the incremental 1 mm distance. Moving across the specimen, the incremental distance was precisely controlled through software by means of an automated stage. For each successive point, the distance and atomic concentration of solute was recorded, and the analysis concluded when the chemical analyzer no longer detected solute.

3.2.5 Numerical Analysis

3.2.5.1 The Thin-film Solution – Disk at One End Equation

The thin-film solution – disk at one end equation, was used for numerical analysis of the data. Equation (6) defines the concentration along a capillary for the case of a thin disk of solute placed at one end. The length of solute particle was very small and could not be measured accurately. However, the weight of the solute particle could be accurately determined and knowing the density of the liquid solute the length of the particle, once melted, could be accurately calculated. If w is the weight of the solute particle, ρ_{lsu} its liquid density and d the capillary diameter, then b is given by $b = 4w / \rho_{lsu} \pi d^2$. Equation (6) then becomes

$$c(x, t) = \frac{4wc_0}{\rho_{lsu} \pi d^2 \sqrt{\pi Dt}} e^{\left[\frac{-x^2}{4Dt} \right]} \quad (49)$$

The experimental diffusion coefficient D_{Exp} for a given time and temperature was determined using Equation (49) by first acquiring a concentration (at%) versus distance (cm) plot from the sample, and then iterating through various diffusion coefficients until a best fit curve (method of least squares) was generated.

A second set of solutions occur by taking the natural logarithm of Equation (49) in which a linear relationship develops that can be used to validate the curve fit value of D_{Exp} . This is given by Equations (50) through (52),

$$\ln(c) = \left[\ln \frac{4wc_0}{\rho_{isu}\pi d^2 \sqrt{\pi Dt}} \right] + \left[\frac{-x^2}{4Dt} \right] = A + x^2 B \quad (50)$$

where A is the value of the intercept and B is the negative slope of a plot $\ln [c(x,t)]$ vs. x^2 .

From Equation (50), the value of the diffusion coefficient can also be determined from the value of the intercept, D_{Int} , via

$$D_{Int} = \left[\frac{1}{\pi t} \right] \left[\frac{4wc_0}{\rho_{isu}\pi d^2 \exp(A)} \right]^2 \quad (51)$$

Similarly, the value of the diffusion coefficient can be determined from the value of the slope, B , in Equation (50) via

$$D_{Slope} = \frac{-1}{B4t} \quad (52)$$

Determining the value of the interdiffusion coefficient in three ways provides excellent confirmation of the results.

3.2.5.2 *Data Normalization*

An important consequence of the solute disk long capillary method is that the total amount of solute remains fixed throughout the diffusion experiment. In an experimental c vs. x plot, the area bound by the curve is proportional to the initial film length. This offers a quantitative check for experimental findings via the relationship

$$\int_0^{\infty} c(x,t)dx = bc_o . \quad (53)$$

By accurately measuring the mass of the cylindrical solute film, a ratio of the area to the product of the initial concentration by the film length can be calculated. Because the graphite capillary is fully sealed, no mass can escape during experimentation and the ratio should be unity. Any deviation from the ideal for reasonable experimental plots can only be attributed to an inaccurate initial mass measurement, or failure of the EDS software to accurately measure the atomic concentration due to the presence of background noise. It was assumed in the analysis that if the diffusion curve followed the thin-film equation with low error, no mass had been lost.

3.2.5.3 *The Experimental Diffusion Coefficient*

Theoretically, all three thin-film solutions should be identical if the diffusion coefficient D is constant and does not vary with concentration, and in fact, the three calculated

values of D usually agreed to within 25%. However, a decision was made to use the diffusion coefficient D_{Exp} produced from the best fit exponential solution, for this value was less sensitive to the effect of increased fluctuations at lower concentration. Both D_{Int} and D_{Slope} are included in Appendix A for reference.

It should be noted that most other investigators use only the slope method to calculate the diffusion coefficient, and thus do not utilize all the information available from the experimental results.

3.2.5.4 Limits of Error

The error limits of the diffusion coefficients were determined using linear and nonlinear least squares regression analysis via the statistical software packages SPSS 16 and Microsoft Excel 2003.

For nonlinear least squares regression, SPSS 16 produced a value for D_{Exp} with a corresponding standard error which satisfies Equation (49). The standard error was taken as the upper and lower error limit.

For linear least squares regression, Microsoft Excel 2003 produced values for coefficients A and B (with corresponding standard errors) which satisfied Equation (50). From coefficients A and B , D_{Int} and D_{Slope} were calculated using Equations (51) and (52). The upper and lower error limits for the diffusion coefficients were taken to be the difference

between the values produced from coefficients A & B, and A & B plus/minus the standard error.

4 EXPERIMENTAL RESULTS

The following tables present the experimental diffusion coefficient D_{Exp} , as determined by Equation (49). A summary of the complete data set, which includes diffusion coefficients calculated using the slope (D_{Slope}) and intercept (D_{Int}) solutions of Equation (51) and (52), is located in Appendix A of this thesis.

4.1 Bismuth in Tin – Summary of Experimental Data

Table 3. Liquid diffusion of Bi in Sn – 0.5 mm capillary diameter dataset.

Temperature (K)	Capillary Diameter (mm)	Time (h)	Experimental Diffusion Coefficient D_{Exp} ($m^2/s \times 10^9$)		
573	0.5	3	2.47	+/-	0.06
573	0.5	3	2.62	+/-	0.05
673	0.5	3	2.29	+/-	0.07
673	0.5	3	1.98	+/-	0.06
773	0.5	3	3.28	+/-	0.20
773	0.5	3	3.79	+/-	0.08
873	0.5	3	4.78	+/-	0.06
873	0.5	3	4.17	+/-	0.09
973	0.5	3	6.17	+/-	0.15
973	0.5	3	7.14	+/-	0.20
1073	0.5	1.5	26.50	+/-	0.93

Table 4. Liquid diffusion of Bi in Sn – 0.8 mm capillary diameter dataset.

Temperature (K)	Capillary Diameter (mm)	Time (h)	Experimental Diffusion Coefficient D_{Exp} ($m^2/s \times 10^9$)		
673	0.8	3	3.05	+/-	0.12
673	0.8	3	3.03	+/-	0.16
773	0.8	3	3.56	+/-	0.08
773	0.8	3	3.18	+/-	0.08
873	0.8	3	4.19	+/-	0.16
873	0.8	3	6.19	+/-	0.22
973	0.8	3	6.41	+/-	0.29
973	0.8	3	6.69	+/-	0.36
1073	0.8	3	8.99	+/-	1.16
1073	0.8	3	11.51	+/-	0.90

Table 5. Liquid diffusion of Bi in Sn – 1.6 mm capillary diameter dataset.

Temperature (K)	Capillary Diameter (mm)	Time (h)	Experimental Diffusion Coefficient D_{Exp} ($m^2/s \times 10^9$)		
773	1.6	6	3.93	+/-	0.06
773	1.6	6	4.41	+/-	0.08
773	1.6	6	4.19	+/-	0.08
773	1.6	6	4.42	+/-	0.07
873	1.6	6	5.20	+/-	0.08
873	1.6	6	4.82	+/-	0.09
973	1.6	6	7.48	+/-	0.14
973	1.6	6	15.85	+/-	0.68
973	1.6	6	16.24	+/-	0.74

4.2 Zinc in Tin - Summary of Experimental Data

Table 6. Liquid diffusion of Zn in Sn – 0.5 mm capillary diameter dataset.

Temperature (K)	Capillary Diameter (mm)	Time (h)	Experimental Diffusion Coefficient D_{Exp} ($m^2/s \times 10^9$)		
723	0.5	2.5	4.51	+/-	0.13
723	0.5	2.5	4.28	+/-	0.12
773	0.5	2.5	5.34	+/-	0.14
773	0.5	2.5	4.13	+/-	0.12
773	0.5	2	4.58	+/-	0.20
823	0.5	2	4.55	+/-	0.17
823	0.5	2	4.47	+/-	0.34
873	0.5	2	5.31	+/-	0.54
873	0.5	2	5.82	+/-	0.28

Table 7. Liquid diffusion of Zn in Sn – 1.6 mm capillary diameter dataset.

Temperature (K)	Capillary Diameter (mm)	Time (h)	Experimental Diffusion Coefficient D_{Exp} ($m^2/s \times 10^9$)		
873	1.6	3	9.52	+/-	1.07
873	1.6	3	8.86	+/-	0.70

5 DISCUSSION

5.1 Arrhenius Analysis

In Figure 11, the Bi in Sn interdiffusion data of Tables 3, 4, and 5 are presented. The figure offers four separate data series, including a series for each capillary diameter tested and a suggested best fit Arrhenius line for Bi-Sn interdiffusion. The observable trend in this figure is that the diffusion coefficient grows larger with both increasing temperature and increasing capillary diameter, noting that some exceptions occur.

For the temperature range of $1/T=0.00175$ (573 K) to $1/T=0.00103$ (973 K), experiments

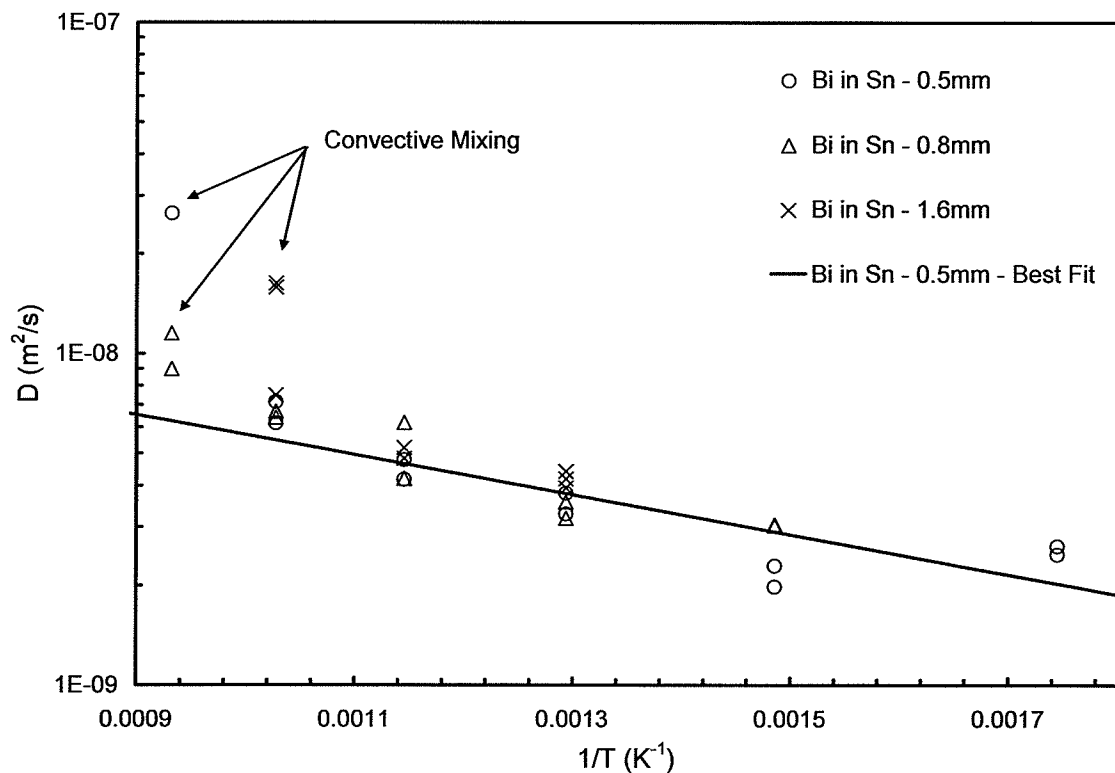


Figure 11. Arrhenius plot for the interdiffusion of Bi in liquid Sn.

utilizing 0.5 mm capillaries consistently produce diffusion coefficients of the lowest value and error for a specified temperature. For this reason, the 0.5 mm data series is curve fit using an Arrhenius relationship to produce parameters which can be compared to literature. The least squares regression analysis yields best fit values for the activation energy of $Q = 11.56 \pm 2.39$ kJ/mole, with a frequency factor of $D_0 = 2.29 \pm 0.74 \times 10^{-8}$ m²/s. (Note: The result obtained at 1073 K is subject to convective mixing and has not been included in the best fit analysis.)

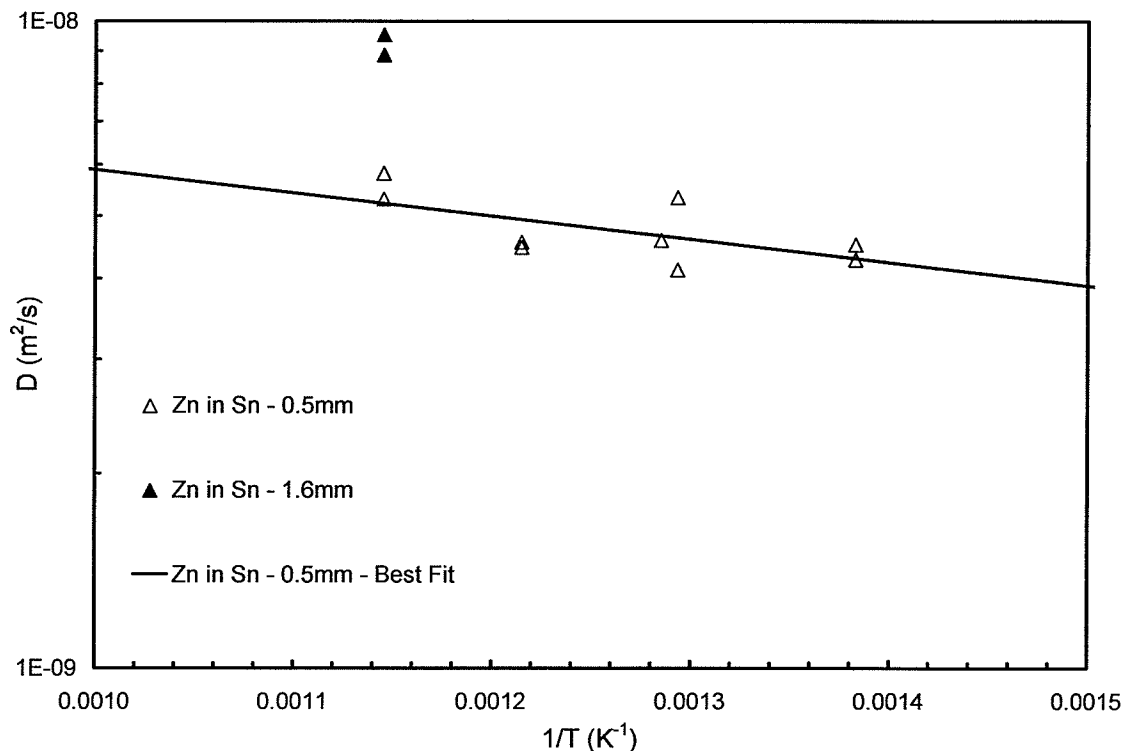


Figure 12. Arrhenius plot for the interdiffusion of Zn in liquid Sn.

In Figure 12, the Zn in Sn interdiffusion data of Tables 6 and 7 are presented. The figure exhibits three separate data series, including a series for each capillary diameter tested

and a best fit Arrhenius line for Zn-Sn interdiffusion. Again, an observable trend in this figure is that the diffusion coefficient grows larger with both increasing temperature and increasing capillary diameter. Least squares regression analysis of the 0.5 mm capillary data series yields best fit values for the activation energy of $Q = 6.86 \pm 3.17$ kJ/mole, with a frequency factor of $D_0 = 1.34 \pm 0.83 \times 10^{-8}$ m²/s.

5.2 Tin Solvent Self Diffusion – A Comparison of Best Fit Experimental Data

Cahoon et al.^[26] using an extensive list of investigations, calculated Arrhenius best fit parameters for the solvent self diffusion of Sn of $Q = 12.10 \pm 0.37$ kJ/mole and $D_o = 3.49 \pm 0.22 \times 10^{-8}$ m²/s (Figure 7). In Figure 13, the best fit Sn solvent self diffusion Arrhenius profile is compared to the Bi-Sn interdiffusion data of this study. It is apparent from the figure that Bi diffuses slower than Sn in liquid Sn at temperatures less than $1/T = 0.00103$ (973 K).

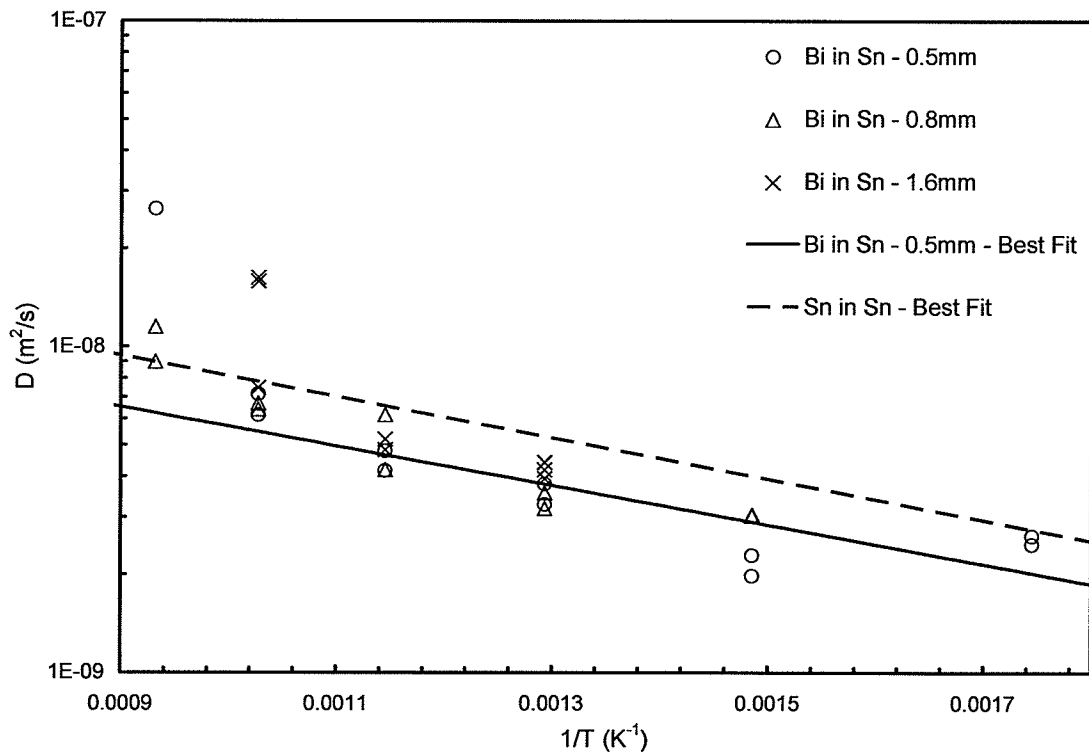


Figure 13. Comparison of 0.5-mm Bi in Sn Experimental Results and Best Fit Sn Solvent Self-Diffusion Data.

In Figure 14, the best fit Sn solvent self diffusion Arrhenius profile is plotted against the Zn-Sn interdiffusion data of this study. At $1/T = 0.00138$ (723 K), Zn diffuses at the same

rate as Sn in liquid Sn, but appears to diffuse slower than Sn over the temperature range of $1/T=0.00129$ (773 K) to $1/T=0.00115$ (873 K).

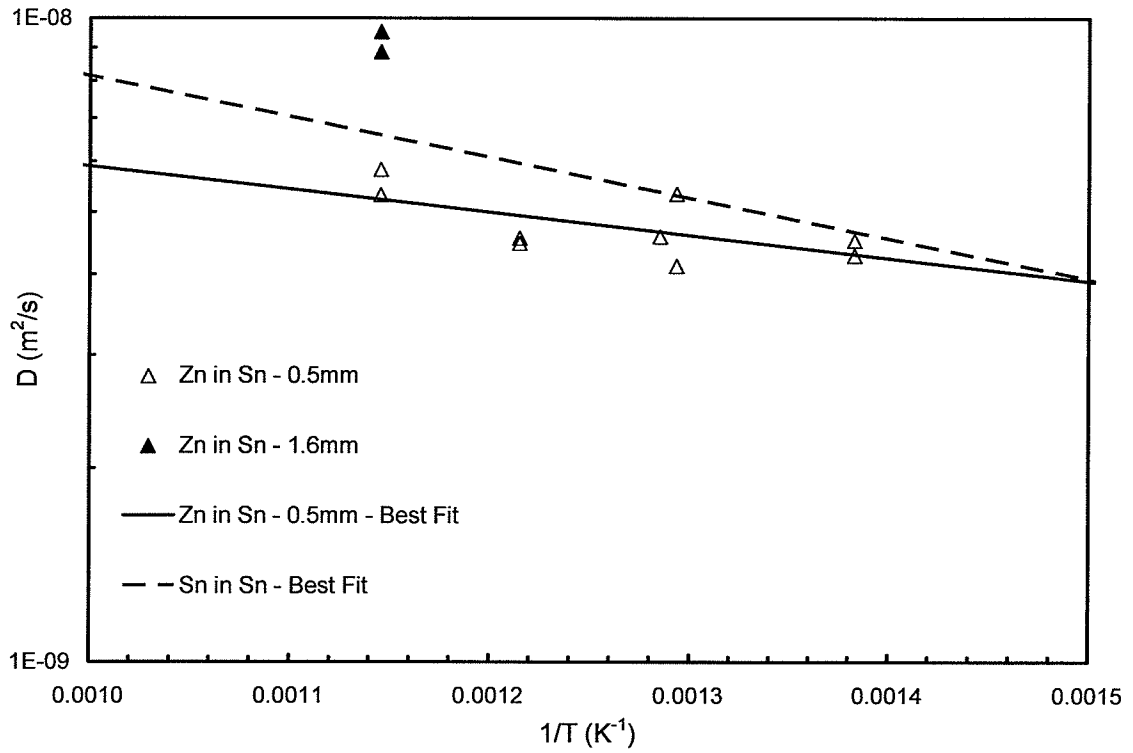


Figure 14. Comparison of 0.5-mm Zn in Sn Experimental Results and Best Fit Sn Solvent Self-Diffusion Data.

Several articles question the validity of diffusion coefficients obtained using the capillary reservoir and shear cell experimental techniques, stating that both methods are subject to error. In their paper, Cahoon et al. ^[6] suggest that:

“...for the capillary-reservoir technique, convective flow in the reservoir across the open end of the capillaries induces “lid-driven” flow in the upper portions of the capillaries, resulting in higher than actual diffusion coefficients, particularly for the Sn-rich alloys, since the Sn-rich end of the capillaries was open to the reservoir.”

Similarly, Masaki et al. ^[42] discuss sources of error in the shear cell method, stating the:

“...problem is unavoidable for the shear cell method. The rotation of the cell added a drag force to the liquid at the contact with the moving disc and a pair of small vortex flows occurs on the joining of liquids, therefore, the step function of the solute distribution as the initial solute distribution is destroyed because a small amount of volume exchange occurs between each liquid piece of diffusion couple. This error of concentration in the initial stage provides an additional contribution of errors to the evaluation of the true diffusion coefficient.”

In addition, diffusion coefficients produced using a shear cell may be influenced by mass transport as a result of free surface Marangoni convection. ^[43, 44]

The 0.5 mm capillary diameter interdiffusion coefficients of Zn in Sn are also in agreement with values found in literature. In Figure 16, a direct comparison of values determined by this study can be made with the long capillary results of Cahoon et al. [26], which were determined using a 1.6 mm diameter capillary.

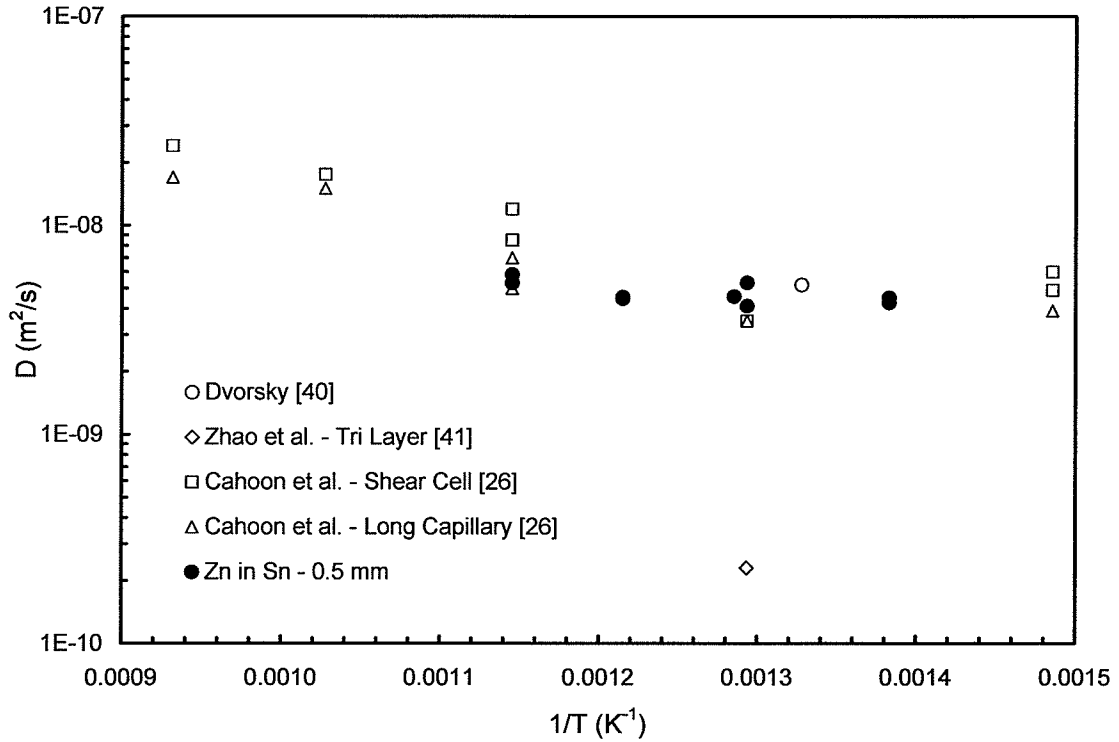


Figure 16. Comparison of the best fit 0.5-mm Zn in Sn experimental results and published Bi in Sn liquid diffusion studies.

5.4 The Effect of Capillary Diameter on the Diffusion Coefficient

The effect of capillary diameter on the diffusion coefficient is visually evident in the Bi-Sn concentration versus distance profiles, presented in the following figures at 973 K for capillary diameters of 1.6 mm, 0.8 mm, and 0.5 mm.

As most apparent in Figure 17, as convection starts, the concentration profile begins to show scatter. Initially, the convection is localized over short distances and does not greatly affect the overall diffusion coefficient; but as convection increases, the

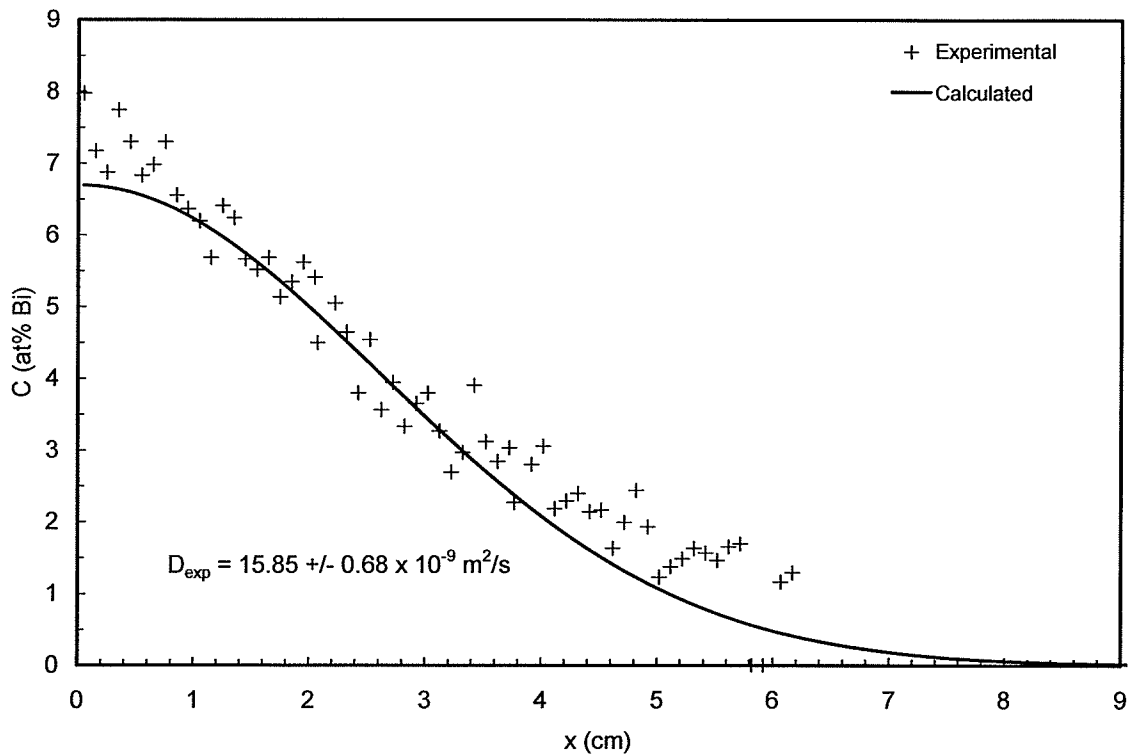


Figure 17. The best curve fit for the thin-film diffusion of Bi in Sn in a 1.6 mm diameter capillary after 6 hours at 973 K.

concentration profile is affected over increasing distances causing a large change in the apparent diffusion coefficient. Although the diffusive profile was curve fit using the thin-film equation, the resulting value of the experimental diffusion coefficient is both inflated and erroneous in comparison to the 0.8 mm and 0.5 mm results.

This phenomena was also reported by Froberg et al. ^[45], for In – Sn diffusion specimens annealed over the range of 533 K to 1173 K. In their study, which utilized 2 mm graphite capillaries, diffusion coefficients were 15 to 30 percent larger than values obtained in microgravity. The concentration versus distance plots for In – Sn exhibited the same

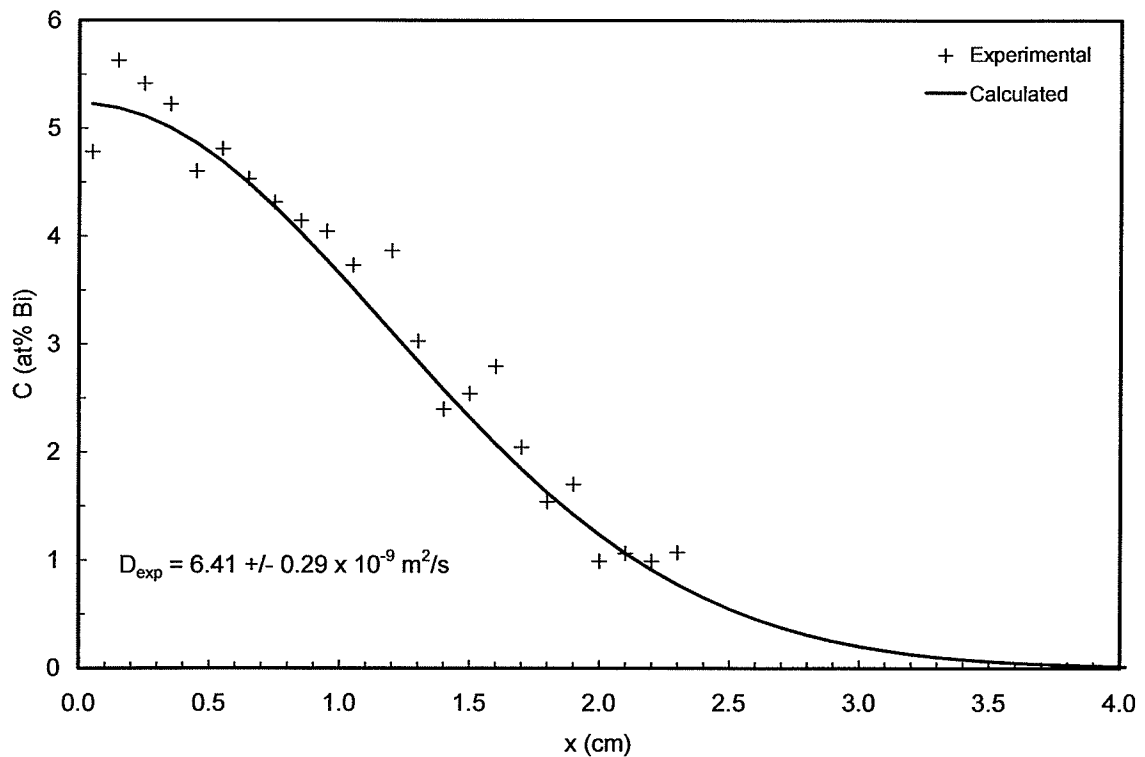


Figure 18. The best curve fit for the thin-film diffusion of Bi in Sn in a 0.8 mm diameter capillary after 3 hours at 973 K.

band of scatter as depicted in Figure 17, which Frohberg et al. also attributed to the effects of convection.

In Figure 18, at the 0.8 mm capillary diameter, the diffusion profile becomes more defined as less scatter is evident. It appears that a reduction in capillary diameter stabilizes the convective currents within the liquid, and as result, the diffusion coefficient decreases and exhibits less error.

This trend is further exemplified as the capillary diameter decreases to 0.5 mm. Although

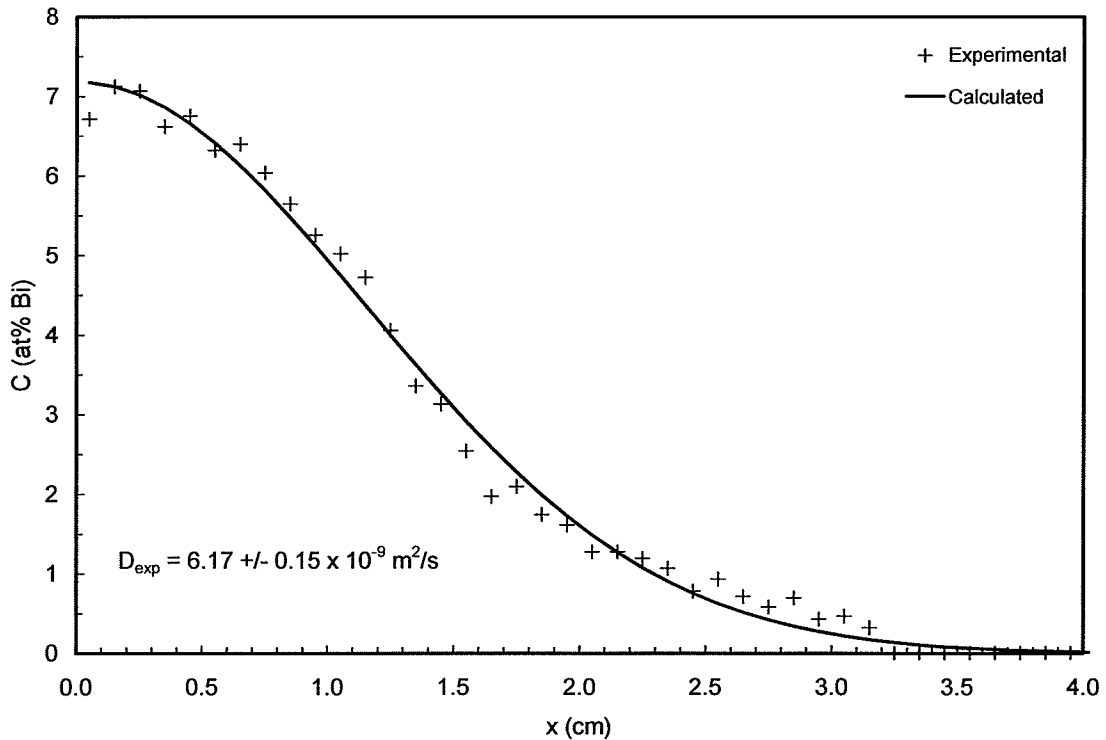


Figure 19. The best curve fit for the thin-film diffusion of Bi in Sn in a 0.5 mm diameter capillary after 3 hours at 973 K.

the experimental diffusion coefficient decreases only slightly, the diffusion profile at 0.5 mm is now well defined and less subject to scatter as shown in Figure 19.

Overall, for Bi-Sn the 1.6 mm capillary yields a diffusion coefficient approximately 250% greater than the identical experiment performed within a 0.5 mm capillary. Though interestingly, at a lower temperature of 873 K for Zn-Sn, the diffusion profile still appears to display localized density fluctuations at 0.5 mm (Figures 20 – 21), suggesting that the ideal capillary diameter for experimentation varies with the choice of solute for Sn interdiffusion.

Lee et al. ^[46] reported similar findings in their investigation of the Al-Cu system using Alumina long capillaries. In a systematic study, samples of different diameters were directionally solidified, and the diffusion coefficient was determined from the measurement of the composition profile ahead of the quenched planar interface. They determined that a critical diameter of 0.8 mm is required to suppress fluid flow within the liquid. “We have shown that the scatter in the data is not random, but the measured values increased systematically as the diameter of the sample used in the experiments was increased.”

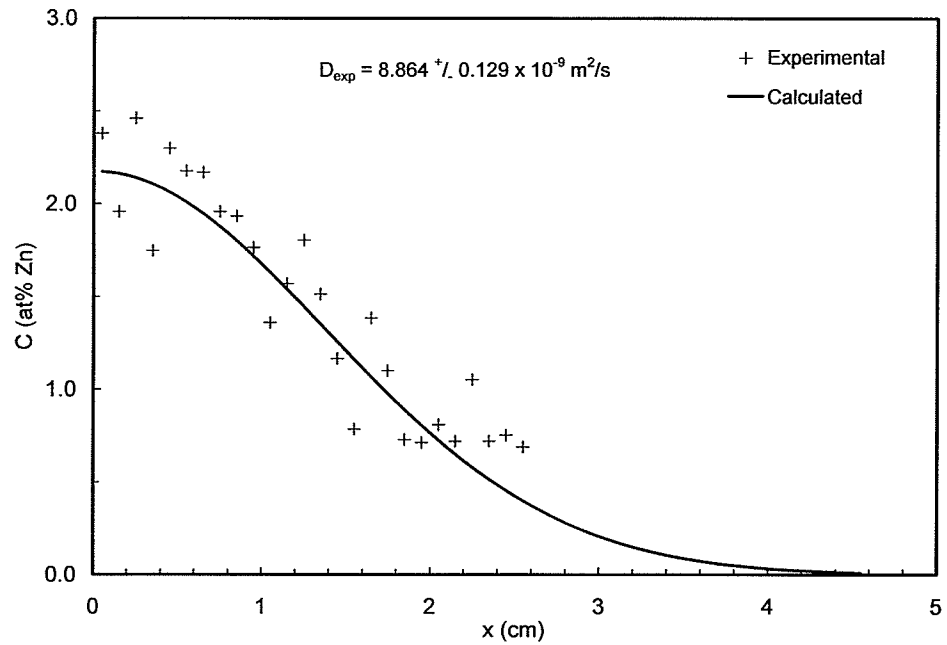


Figure 20. The best curve fit for the thin-film diffusion of Zn in Sn in a 1.6 mm diameter capillary after 3 hours at 873 K.

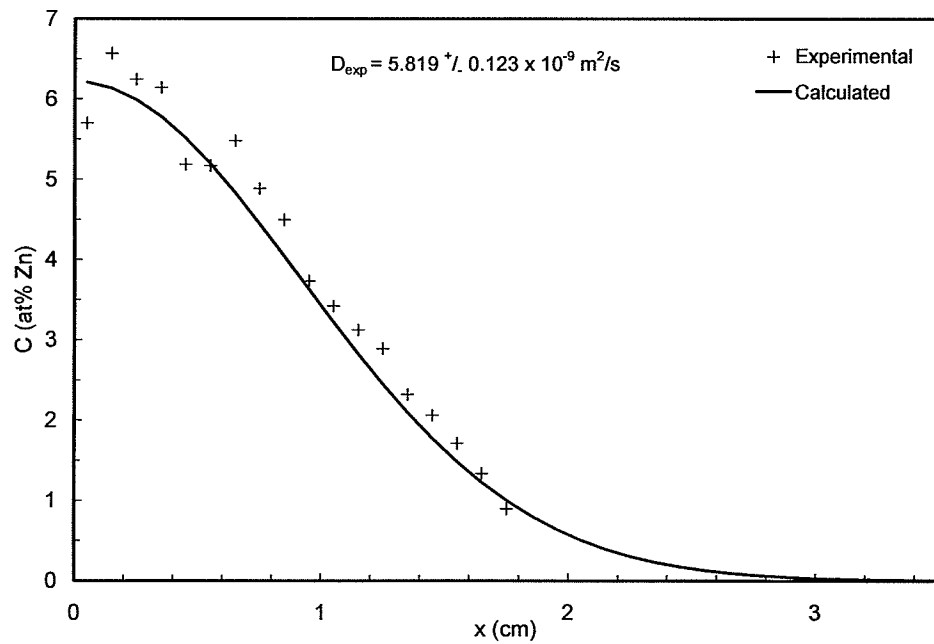


Figure 21. The best curve fit for the thin-film diffusion of Zn in Sn in a 0.5 mm diameter capillary after 3 hours at 873 K.

5.5 Scaling and Numerical Analysis

The scaling and numerical analysis developed by Garandet et al. ^[25], as discussed in section 2.5 *The Effect of Capillary Diameter on the Diffusion Coefficient*, is applied to the findings of this study for diffusion of Bi in Sn at 873 K and 973 K in Figures 22 and 23 respectively. In this analysis, the horizontal temperature difference ΔT_H is taken to be 0.2 K / mm, while the remaining parameters are defined in *APPENDIX B – Select Physical Properties of Tin, Zinc and Bismuth*.

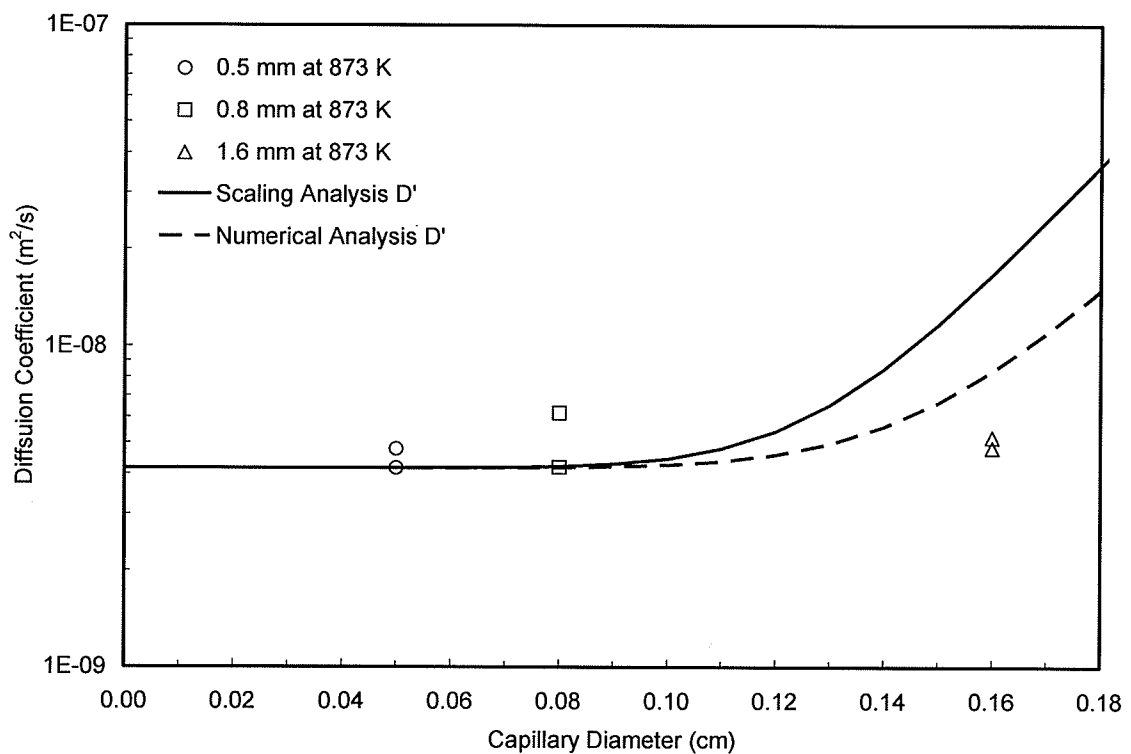


Figure 22. The apparent diffusion coefficient for diffusion of Bi in Sn as defined by the scaling and numerical analyses of Garandet et al. ^[25] as function of the capillary diameter, compared to results obtained in this study at 873 K.

At 873 K, the size of the capillary diameter seems to have little effect on the experimental diffusion coefficient, but both the scaling and numerical analysis predict that the diffusion coefficient should begin to increase at capillary diameters in excess of 0.8 mm.

Interestingly, at 973 K (Figure 23), the scaling analysis seems to accurately predict the increase in the rate of diffusion within the 1.6 mm capillary. As previously discussed, it was not until 973 K that convective mixing became evident in the experimental data.

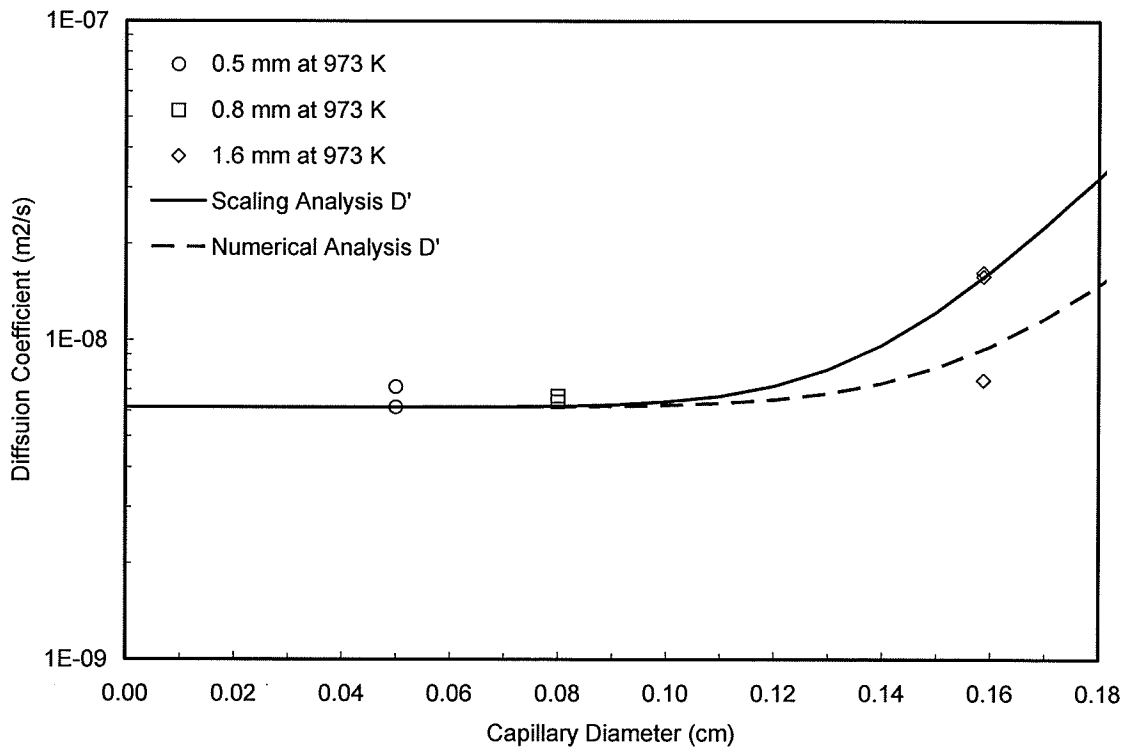


Figure 23. The apparent diffusion coefficient on Bi in Sn as defined by the scaling and numerical analyses of Garandet et al. ^[25] as function of the capillary diameter, compared to results obtained in this study at 973 K.

In a similar investigation, Müller et al. ^[43] applied the scaling analysis to the interdiffusion of Sn in In at 673 K, but did not observe the same correlation. Their analysis utilized a data set compiled from 29 experiments performed on earth using a shear cell, and a value determined in microgravity as base reference. Interestingly, they observed considerable variation in the diffusion coefficient at capillary diameters of 0.7 mm and 1.0 mm, which is not predicted by the scaling analysis, and is not in keeping with trends observed in this thesis.

5.6 Possibility of a Liquid Phase Transformation

In the past there has been considerable emphasis upon determining the temperature dependence of liquid diffusion coefficients as indicated in the Theory section of this thesis. It is however possible, that there may be no simple temperature dependence of the diffusion coefficient in at least some liquid alloy metals. For example, recent investigations have suggested that liquid Sn undergoes a “phase transformation” at 673 K^[47] or 773 K^[48], and any such structural change would almost certainly affect the liquid diffusion coefficient. The present study lends some support to this suggestion in that the diffusion coefficient of Zn in liquid Sn (Figure 12) appears lower at $1/T=0.00138$ (723 K) than at $1/T=0.00129$ (773 K). Similarly, the diffusion coefficient of Bi in liquid Sn (Figure 11) appears lower at $1/T=0.00149$ (673 K) than at $1/T=0.00175$ (573 K). Therefore, there may exist some structural change in liquid Sn alloys occurring at a temperature in the range of 600 K – 800 K that would influence the diffusion coefficient.

Structural changes may also occur in other liquid elements. An anomaly in the properties of supercooled liquid silicon has been reported but the nature of the change is unclear^[49].

It is apparent that the study of diffusion in liquid metals is very difficult with many factors to be considered.

6 CONCLUSIONS

In this thesis, a data set for the interdiffusion of the binary Bi-Sn and Zn-Sn systems was determined by optimizing the thin-film long capillary experimental method. From the data set, several conclusions are drawn.

1. The value for the liquid diffusion coefficient of Bi in Sn as determined by the present investigation is given by

$$D_{Bi-Sn} = 11.56 \pm 2.39 \times 10^{-8} \exp \left(- (2.29 \pm 0.74) / RT \right) \text{ m}^2/\text{s}.$$

2. The value for the liquid diffusion coefficient of Zn in Sn as determined by the present investigation is given by

$$D_{Zn-Sn} = 1.34 \pm 0.83 \times 10^{-8} \exp \left(- (6.86 \pm 3.17) / RT \right) \text{ m}^2/\text{s}.$$

3. The diffusion of Bi in Sn is slower than solvent self diffusion of Sn at temperatures less than 1073 K.
4. The diffusion of Zn in Sn is slower than solvent self diffusion of Sn over the temperature range of 773 K to 873 K.
5. The thin-film long capillary method is most effective at a diameter of 0.5 mm. It is proven to lower diffusion coefficients at elevated anneal temperatures, and produce

results in keeping with experiments conducted in microgravity. The reduction capillary diameter appears to stabilize convective mixing, and yield diffusion profiles of greater accuracy. This offers a viable experimental procedure which can be used to produce accurate liquid diffusion coefficients in terrestrial environments.

6. While it may be possible to obtain accurate liquid diffusion coefficients using 0.5 mm diameter capillaries, the diffusion coefficient may be affected by phase transformations or other structural changes in some liquids.

7 RECOMMENDATIONS FOR FUTURE WORK

At the completion of this thesis, several recommendations can be made regarding future work in this research area. These recommendations are listed below.

1. Investigate the possibility of liquid phase transformations within liquid tin, tin-bismuth alloys, and tin-zinc alloys. This could be accomplished by means of differential scanning calorimetry (DCS) or a similar method which is capable of detecting phase transformation across a given temperature range in liquid metals.
2. Perform microgravity experiments for Bi-Sn over the temperature range of 573 K to 1073 K, using both long capillary and shear cell methods.
3. Perform microgravity experiments for Zn-Sn over the temperature range of 723 K to 873 K, using both the long capillary and shear cell methods.
4. Use finite element analysis software to model the effect of diameter on convective flow within the capillary, focusing specifically on the effect of temperature gradients across the capillary diameter.

The experimental results produced by items 1-4 could be directly compared to the findings of this research, and could be used in the development of future a liquid diffusion theory and/or experimental technique.

8 REFERENCES

1. G. Mathiak, E. Plescher and R. Willnecker: Liquid Metal Diffusion Experiments in Microgravity – Vibrational Effects, *Measurement Science and Technology*, 2005, Vol. 16, pp. 336-344.
2. J. Crank: *The Mathematics of Diffusion – 2nd Edition*, 1975, Clarendon Press, Oxford, pp. 2.
3. P. Shewmon: *Diffusion in Solids - 2nd Edition*, 1989, Publication of the Minerals, Metals and Materials Society, Pennsylvania, pp. 10-14.
4. P. Shewmon: *Diffusion in Solids - 2nd Edition*, 1989, Publication of the Minerals, Metals and Materials Society, Pennsylvania, pp. 15-18.
5. P. Shewmon: *Diffusion in Solids - 2nd Edition*, 1989, Publication of the Minerals, Metals and Materials Society, Pennsylvania, pp. 34-36.
6. M. Klassen and J. R. Cahoon: Interdiffusion of Sn and Pb in Liquid Pb-Sn Alloys, *Metallurgical and Materials Transactions A*, 2000, May, Vol. 31A, pp. 1343-1352.
7. J. R. Cahoon: The Entropy Factor in Liquid Diffusion, *Metallurgical and Materials Transactions A*, 2003, March, Vol. 34A, pp. 882-883.
8. R. B. Gordon: Hole Model for Diffusion in Liquids, *Acta Metallurgical*, 1959, Vol. 7, pp. 681-682.
9. W. D. Callister: *Materials Science and Engineering an Introduction - 5th Edition*, 1999, John Wiley & Sons, New York, pp. 102-103.
10. R. A. Swalin: On the Theory of Self-Diffusion in Liquid Metals, *Acta Metallurgica*, 1959, Vol. 7, pp. 736-740.

11. R. A. Swalin and V. G. Leak: Diffusion of Heterovalent Solutes in Liquid Silver, *Acta Metallurgica*, 1965, Vol. 13, pp. 471-478.
12. N. H. Nachtrieb: Self-diffusion in liquid metals, *Advances in Physics*, 1967, Vol. 16, No. 62, pp. 309-322.
13. S. A. Rice and N. H. Nachtrieb: A Comment on Self Diffusion in Liquid Metals, *Advances in Physics*, 1967, Vol. 16, No. 62, pp. 351-356.
14. J. B. Edwards, E. E. Hucke, and J. J. Martin: Diffusion in Binary Liquid Metal Systems, *Metallurgical Reviews*, 1968, Vol. 13, pp. 1-28.
15. F. A. L. Dullien: New Relationship Between Viscosity and the Diffusion Coefficients based on Lamm's Theory of Diffusion, *Trans. Faraday Soc.*, 1963, Vol. 59, pp. 856-868.
16. H. A. Walls and W. R. Upthegrove: Theory of Liquid Diffusion Phenomena, *Acta Metallurgica*, 1964, Vol. 12, pp. 461-471.
17. A. L. Hines and H. A. Walls: Determination of Self Diffusion Coefficients using the Radial Distribution Function, *Met. Trans. A.*, 1979, Vol. 9A, pp. 1365-1370.
18. V. S. Peter: Uber die Viskositat und die Selbstdiffusion von Flussigkeiten, *Z. Naturforschun.*, 1954, Vol. 9a, pp. 98-104.
19. S. Chapman and T. G. Cowling: *The Mathematical Theory of Non-Uniform Gases*, 1953, Cambridge at the University Press.
20. M. Shimoji and T. Itami: Atomic Transport in Liquid Metals, *Diffusion and Defect Data*, Editor-in-Chief, F. H. Wohlbier, 1986, Vol. 43, pp. 1-344.
21. T. Itami, A. Mizuno, and T. Masaki: *Modeling and Precise Experiments of Diffusion Phenomena in Melts Under Microgravity*, *Annual Reports 1998 and 1999, NASDA*

- Technical Memorandum, NASDA-TMR-000013E, National Space Development Agency of Japan*, March 2001, pp. 13-18.
22. M. H. Cohen and D. Turnbull: Molecular Transport in Liquid Glasses, *Journal of Chemical Physics*, 1959, vol. 31, pp. 1164-1169.
23. J. Edwards: *Diffusion in Binary Liquid Metal System*, 1966, University of Michigan, pp. 46.
24. J. D. Verhoeven: Convection Effects in the Capillary Reservoir Technique for Measuring Liquid Metal Diffusion Coefficients, *Transactions of the Metallurgical Society of AIME*, 1968, Vol. 242, pp. 1937-1942.
25. J. P. Garandet, C. Barat, T. Duffar: The Effect of Natural Convection in Mass Transport Measurement in Dilute Liquid Alloys, *International Journal of Heat and Mass Transfer*, 1995, Vol. 38, No. 12, pp. 2169-2174.
26. J. R. Cahoon, Y. Jiao, K. Tandon, and M. Chaturvedi: Interdiffusion of Liquid Tin, *Journal of Phase Equilibria and Diffusion*, 2006, Vol. 27, No. 4, pp. 325-332.
27. U. Soedervall, H. Odelius, A. Lodding, G. Frohberg, K. H. Kraatz, and H. Wever: SIMS Study of Diffusion in Liquid Tin and Associated Isotope Effects, Springer Series in Chemical Physics, *International Conference on Secondary Ion Mass Spectrometry, SIMS 5*, 1986, No. 44, pp. 41-44.
28. A. Bruson and M. Gerl: Diffusion Coefficient of ^{113}Sn , ^{124}Sb , ^{110}Ag , and ^{195}Au in Liquid Sn, *Physical Review B*, 1980, Vol. 21, No. 12, pp. 5447-5454.
29. G. Careri, A. Paoletti, and M. Further: Experiments on Liquid Indium and Tin Self-Diffusion, *Vincentini: Nuovo Cimento*, 1958, Series 10, Vol. 10, pp. 1088-1099.

30. W. Lange, W. Pippel, and H. Opperman: Uber die Bestimmung von Selbst Diffusion Koeffizienten Metalle durch Messung der Radioaktivitat wahrend des Diffusions Prozesses, *Isotopen-Tech*, 1962, Vol. 2, pp. 132-134.
31. K. G. Davis and P. Fryzuk: Application of the Fluctuation Theory of Liquid Diffusion to Self-Diffusion in Liquid Tin, *Journal of Applied Physics*, 1968, Vol. 39, No. 10, pp. 4848-4849.
32. J. P. Foster and R. J. Reynik: Self-Diffusion in Liquid Tin and Indium over Extensive Temperature Ranges, *Metallurgical Transactions B*, 1973, Vol. 4, No. 1, pp. 207-216.
33. Y. I. Khar'kov, A. L. Zvyagintsev, and G. I. Onopriyenko: Self-Diffusion and Diffusion of Impurities in Liquid Tin, *Fiz. Met. Metalloved.*, 1971, Vol. 31, No. 2, pp. 224-225.
34. C. H. Ma and R. A. Swalin: Self-Diffusion in Liquid Tin, *Journal of Chemical Physics*, 1962, Vol. 36, No. 11, pp. 3014-3018.
35. J. D. Verhoeven, E. D. Gibson, and M. B. Beardsley: The Diffusion Coefficient of Bi in Dilute Liquid Alloys of Bi in Sn, *Metallurgical Transactions B*, 1975, June, Vol. 6B, pp. 349.
36. C. H. Buell, and F. O. Shuck: Diffusion in the Liquid Bi-Sn System, *Metallurgical Transactions*, 1970, July, Vol. 1, pp. 1875-1880.
37. R. D. Stover, F.O. Shuck: Diffusion in Liquid Bismuth-Tin Alloys, *Transactions of the Metallurgical Society of AIME*, 1968, Vol. 242, pp. 768-770.
38. Garandet et al.: Measurement of Solute Diffusivities in Liquid Metal Alloys within the AGAT Facility During the FOTON 12 Mission, *Microgravity and Space Station Utilization*, 2000, Vol. 1, No. 4, pp. 29-34.

39. S. Suzuki, K. H. Kraatz, and G. Froberg: Diffusion Experiments in Liquid Sn-Bi and Al-Ni Systems with a Stable Density Layering Using FOTON Shear Cell Under 1G Conditions, *Microgravity Science and Technology*, 2005, Vol. 15, No. 1, pp. 120-126.
40. R. Dvorsky: Difuze Sn A Zn V TAVENINACH ZnSn PRI 480 °C, *Kovove Materialy*, 1988, Vol. 25, No. 1, pp. 125-128.
41. J. Zhao, R. Liu, M. Zhang, Z. Zhou, X. Zhang, L. Cao, D. Dai, Y. Xu, W. Wang: Determination of Interdiffusion Coefficients of Liquid Zinc and Tin Under Convectionless Conditions, *Applied Physics A*, 2000, Vol. 70, pp. 219-222.
42. T. Masaki, T. Fukazawa, S. Matsumoto, T. Itami, and S. Yoda: Measurements of Diffusion Coefficients of Metallic Melt Under Microgravity – Current Status of the Development of Shear Cell Technique Towards JEM on ISS, *Measurement Science and Technology*, 2005, Vol. 16, pp. 326-335.
43. H. Müller, G. Müller -Vogt: Investigation of Additional Convection Transports in Liquid Metals and Semiconductors During Diffusion Measurements by Means of the Shear Cell Technique, *Cryst. Res. Technol.*, 2003, Vol. 38, No. 7-8, pp. 707-715.
44. G. Mathiak, A. Griesche, K.H. Kraatz, G. Froberg: Diffusion in Liquid Metals, *Journal of Non-Crystalline Solids*, 1996, p 412-416.
45. G. Froberg, K. H. Kraatz, H. Wever, A. Lodding, and H. Odelius: Diffusion in Liquid Alloys Under Microgravity, *Defect and Diffusion Forum*, 1989, Vol. 66-69, pp. 295-300.
46. J. H. Lee, Shan Liu, H. Miyahara, and R. Trivedi: Diffusion-Coefficient Measurements in Liquid Metallic Alloys, *Material Transactions B*, 2004, Vol. 35B, pp. 909-917.

47. L. Wang, X. Bian, J. Liu: Discontinuous Structural Phase Transition of Liquid Metal and Alloys (1), *Physics Letters A*, 2004, Vol. 326, pp. 429-435.
48. A. Wu, L. Guo, C. Liu, E. Jia, Z. Zhu: Internal Friction Behavior of Bi-Sn Alloys, *Physica B*, 2005, Vol. 369, pp. 51-55.
49. T. Kim, A. Goldman, K. Kelton: Structural Study of Supercooled Liquid Silicon, *Philosophical Magazine*, 2008, Vol. 88, No. 2, pp. 171-179.
50. *WebElements Periodic Table of the Elements*. Retrieved July 14, 2008, from <http://www.webelements.com/tin/physics.html>.
51. Metals Handbook Ninth Edition – Volume 2 Properties and Selection: Nonferrous Alloys and Pure Metals, *American Society for Metals*, 1979, pp. 811-814.
52. *WebElements Periodic Table of the Elements*. Retrieved July 14, 2008, from <http://www.webelements.com/bismuth/physics.html>.
53. *WebElements Periodic Table of the Elements*. Retrieved July 14, 2008, from <http://www.webelements.com/zinc/physics.html>.
54. ASM Handbook - Volume 3 Alloy Phase Diagrams, *ASM International*, 1992, pp. 2•106.
55. ASM Handbook - Volume 3 Alloy Phase Diagrams, *ASM International*, 1992, pp. 2•372.

9 APPENDIX A – Complete Experimental Dataset

The following tables present a summary of the complete experimental data set of this thesis.

Table 8. Liquid Diffusion of Bismuth in Tin - 0.5 mm Capillary Diameter

Temperature (K)	Time (h)	D_{Exp} ($m^2/s \times 10^9$)	D_{Slope} ($m^2/s \times 10^9$)	D_{int} ($m^2/s \times 10^9$)
573	3	2.47 +/- 0.06	2.37 +/- 0.09	2.26 +/- 0.12
573	3	2.62 +/- 0.05	2.59 +/- 0.03	2.52 +/- 0.05
673	3	2.29 +/- 0.07	2.73 +/- 0.13	2.77 +/- 0.16
673	3	1.98 +/- 0.06	2.25 +/- 0.17	2.34 +/- 0.11
773	3	3.28 +/- 0.20	3.46 +/- 0.30	3.20 +/- 0.20
773	3	3.79 +/- 0.08	3.95 +/- 0.08	3.86 +/- 0.11
873	3	4.78 +/- 0.06	5.09 +/- 0.08	5.05 +/- 0.10
873	3	4.17 +/- 0.09	4.40 +/- 0.07	4.32 +/- 0.09
973	3	6.17 +/- 0.15	7.40 +/- 0.23	7.77 +/- 0.34
973	3	7.14 +/- 0.20	6.80 +/- 0.23	7.14 +/- 0.26
1073	1.5	26.50 +/- 0.93	30.17 +/- 0.99	28.44 +/- 0.96

Table 9. Liquid Diffusion of Bismuth in Tin - 0.8 mm Capillary Diameter

Temperature (K)	Time (h)	D_{Exp} ($m^2/s \times 10^9$)	D_{Slope} ($m^2/s \times 10^9$)	D_{int} ($m^2/s \times 10^9$)
673	3	3.05 +/- 0.12	3.33 +/- 0.13	3.06 +/- 0.10
673	3	3.03 +/- 0.16	3.00 +/- 0.11	2.79 +/- 0.10
773	3	3.56 +/- 0.08	3.66 +/- 0.07	3.62 +/- 0.09
773	3	3.18 +/- 0.08	3.85 +/- 0.15	3.96 +/- 0.19
873	3	4.19 +/- 0.16	4.73 +/- 0.11	4.90 +/- 0.19
873	3	6.19 +/- 0.22	6.98 +/- 0.21	7.25 +/- 0.34
973	3	6.41 +/- 0.29	6.74 +/- 0.31	6.13 +/- 0.24
973	3	6.69 +/- 0.36	8.10 +/- 0.37	6.83 +/- 0.20
1073	3	8.99 +/- 1.16	15.67 +/- 4.13	9.48 +/- 0.43
1073	3	11.52 +/- 0.90	15.57 +/- 1.78	12.29 +/- 0.67

Table 10. Liquid Diffusion of Bismuth in Tin – 1.6 mm Capillary Diameter

Temperature (K)	Time (h)	D_{Exp} ($m^2/s \times 10^9$)	D_{Slope} ($m^2/s \times 10^9$)	D_{int} ($m^2/s \times 10^9$)
773	6	3.93 +/- 0.06	4.05 +/- 0.07	4.05 +/- 0.12
773	6	4.41 +/- 0.08	4.27 +/- 0.08	4.20 +/- 0.11
773	6	4.18 +/- 0.08	4.13 +/- 0.09	4.01 +/- 0.12
773	6	4.42 +/- 0.07	4.57 +/- 0.12	4.67 +/- 0.19
873	6	5.20 +/- 0.08	5.52 +/- 0.13	5.46 +/- 0.18
873	6	4.82 +/- 0.09	5.50 +/- 0.17	5.42 +/- 0.19
973	6	7.48 +/- 0.14	7.54 +/- 0.15	7.09 +/- 0.17
973	6	15.85 +/- 0.68	22.25 +/- 0.90	17.75 +/- 0.54
973	6	16.24 +/- 0.74	20.35 +/- 0.84	16.66 +/- 0.58

Table 11. Liquid Diffusion of Zinc in Tin - 0.5 mm Capillary Diameter

Temperature (K)	Time (h)	D_{Exp} ($m^2/s \times 10^9$)	D_{Slope} ($m^2/s \times 10^9$)	D_{int} ($m^2/s \times 10^9$)
723	2.5	4.51 +/- 0.13	4.29 +/- 0.12	4.09 +/- 0.15
723	2.5	4.28 +/- 0.12	4.03 +/- 0.08	3.87 +/- 0.11
773	2.5	5.34 +/- 0.14	5.82 +/- 0.13	5.50 +/- 0.13
773	2.5	4.12 +/- 0.12	4.16 +/- 0.13	4.02 +/- 0.16
778	2	4.58 +/- 0.20	4.14 +/- 0.15	3.92 +/- 0.70
823	2	4.55 +/- 0.17	4.79 +/- 0.14	4.43 +/- 0.12
823	2	4.47 +/- 0.34	5.22 +/- 0.43	4.44 +/- 0.23
873	2	5.31 +/- 0.54	7.05 +/- 0.96	6.08 +/- 0.48
873	2	5.82 +/- 0.28	5.97 +/- 0.21	5.34 +/- 0.16

Table 12. Liquid Diffusion of Zinc in Tin – 1.6 mm Capillary Diameter

Temperature (K)	Time (h)	D_{Exp} ($m^2/s \times 10^9$)	D_{Slope} ($m^2/s \times 10^9$)	D_{int} ($m^2/s \times 10^9$)
873	3	9.52 +/- 1.07	18.59 +/- 2.81	9.97 +/- 0.36
873	3	8.86 +/- 0.70	11.61 +/- 1.24	9.78 +/- 0.58

10 APPENDIX B – Select Physical Properties of Tin, Zinc and Bismuth

10.1 Tin – Select Physical Properties

Table 13. Select physical properties of Tin. ^[50]

Tin		
Symbol	Sn	
Atomic Number	50	
Molecular Weight	118.710	g/mol
Melting Point	231.968	°C
Boiling Point	2602	°C

Table 14. Numerical values for kinematic viscosity as a function of temperature of liquid Tin. ^[51]

Temperature (K)	Kinematic Viscosity ($\text{m}^2/\text{s} \times 10^7$)
505	3.820
523	2.654
573	2.354
673	1.974
773	1.702
873	1.528
973	1.394
1073	1.288

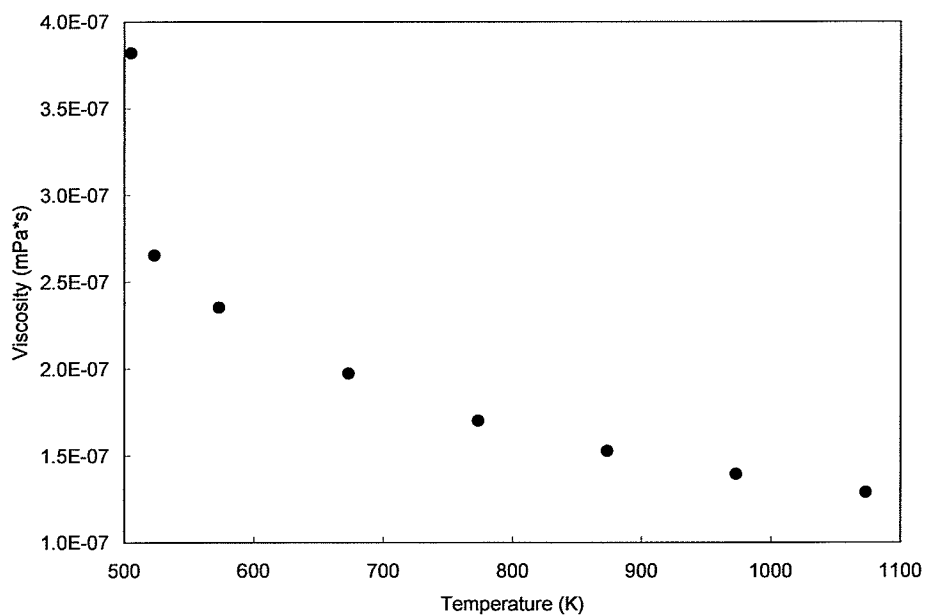


Figure 24. Kinematic viscosity versus temperature for liquid Tin.

Table 15. Numerical values for density as a function of temperature for liquid Tin.

[51]

Temperature (K)	Density (Mg/m ³)
571	6.940
682	6.840
747	6.789
796	6.761
811	6.770
847	6.729
875	6.711
921	6.671
1089	6.620
1366	6.450
1644	6.290
1846	6.160

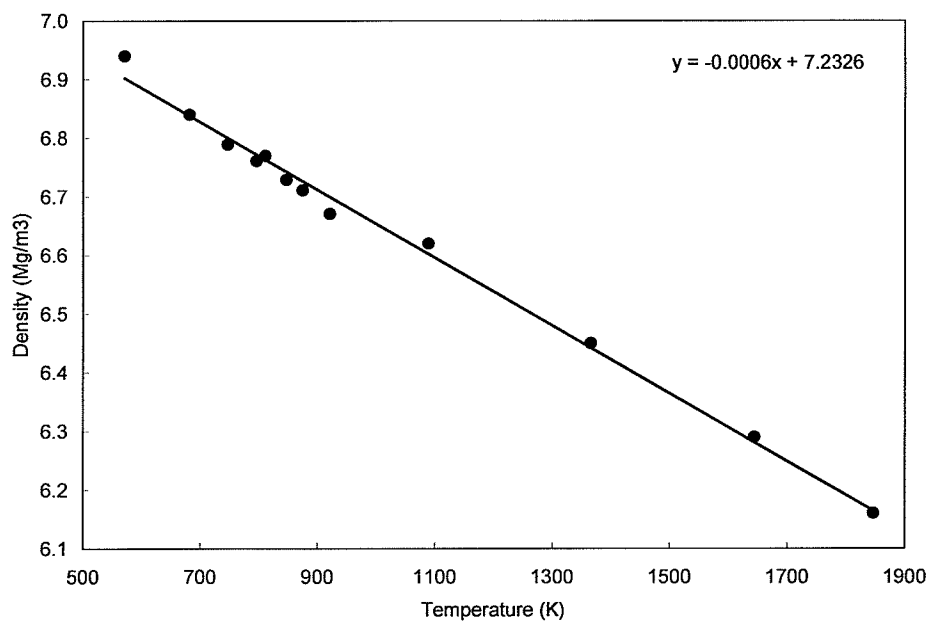


Figure 25. Density versus temperature for liquid Tin.

10.2 Bismuth – Select Physical Properties

Table 16. Select physical properties of Bismuth. ^[52]

Bismuth		
Symbol	Bi	
Atomic Number	83	
Molecular Weight	208.980	g/mol
Melting Point	271.3	°C
Boiling Point	1564	°C
Density	9.80	g / cm ³

10.3 Zinc – Select Physical Properties

Table 17. Select physical properties of Zinc. ^[53]

Zinc		
Symbol	Zn	
Atomic Number	30	
Molecular Weight	65.409	g/mol
Melting Point	419.58	°C
Boiling Point	907.00	°C
Density	7.10	g / cm ³

10.4 Bismuth-Tin Binary Phase Diagram

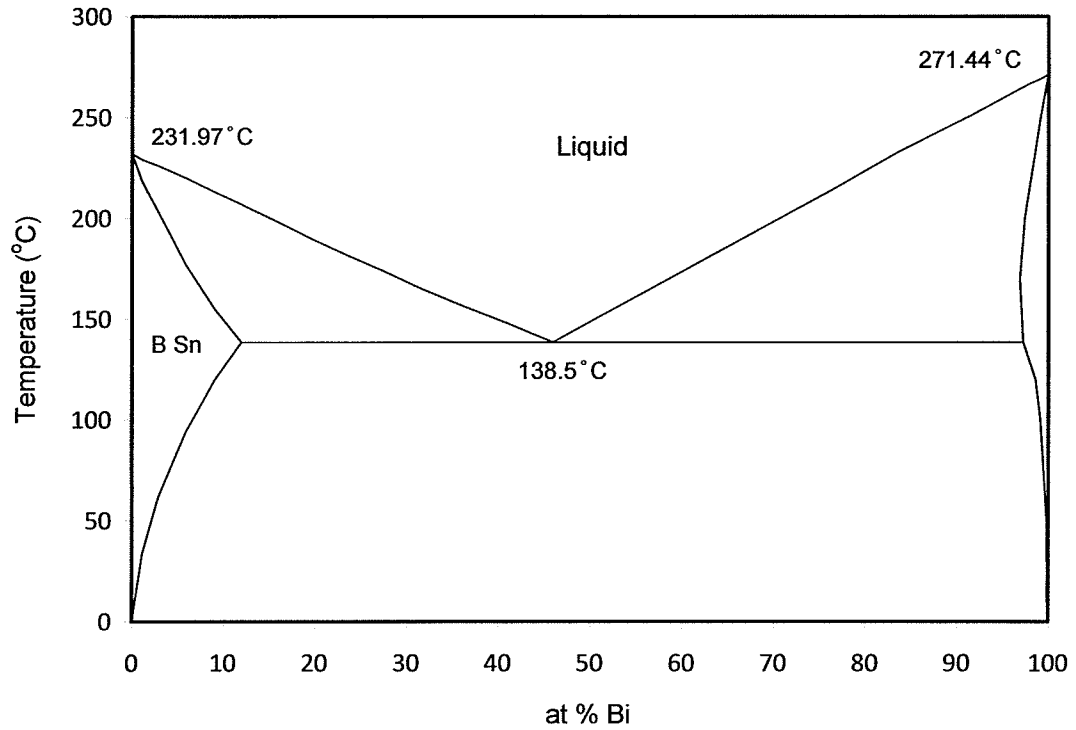


Figure 26. Bismuth in Tin Binary Phase Diagram – Atomic Percent Bismuth versus Temperature. [54]

10.5 Tin-Zinc Binary Phase Diagram

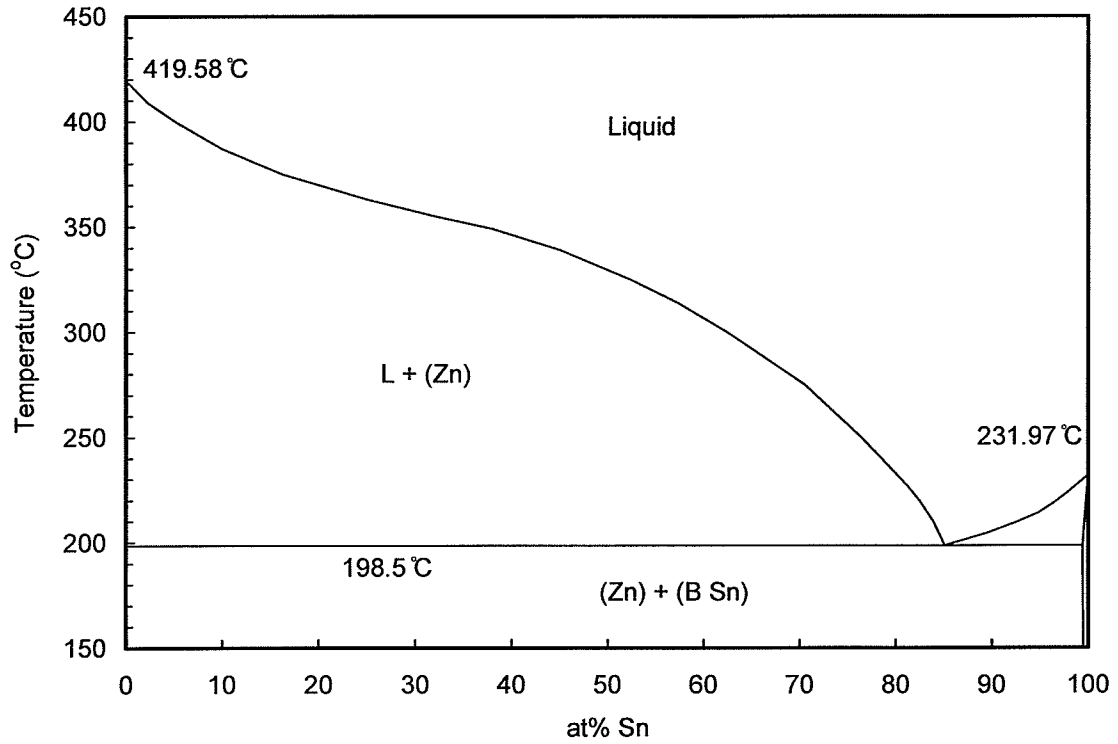


Figure 27. Tin in Zinc Binary Phase Diagram – Atomic Percent Tin versus Temperature. ^[55]